INTEGRATION OF RED & BLUE TL MATERIALS TO DIFFERENT POLYMER END-USE

A Thesis Submitted to
the Graduate School of Engineering and Sciences of
İzmir Institute of Technology
in Partial Fulfillment of the Requirements for the Degree of

MASTER OF SCIENCE

in Materials Science and Engineering

by

ANIL İNCEL

July 2016

İZMİR

We approve the thesis of **Anıl İNCEL**

Examining Committee Members:

Prof. Dr. Mustafa M. DEMİR
Department of Materials Science and Engineering, İzmir Institute of Technology

Assoc. Prof. Dr. Ali Çağır
Department of Chemistry, İzmir Institute of Technology

Assoc. Prof. Volkan Çeçen
Bergama Vocational School, Dokuz Eylül Üniversity

25 July 2016

Prof. Dr. Mustafa M. DEMİR
Supervisor, Department of Materials Science and Engineering
İzmir Institute of Technology

Assist. Prof. Engin Karabudak
Co-Supervisor, Department of Chemistry
İzmir Institute of Techology

Prof. Dr. Mustafa M. DEMİR
Head of the Department of Materials Science and Engineering

Prof. Dr. Bilge KARAÇALI
Dean of the Graduate School of Engineering and Sciences

ACKNOWLEDGEMENTS

I would never have been able to finish my thesis without the guidance of my committee members, help from friends, and support from my family.

Firstly, I would like to express my deepest gratitude to my advisor, Prof. Mustafa M. Demir, for his excellent guidance, caring, patience, confidence and providing me with an excellent atmosphere for doing this research. I could not have imagined having a better and friendlier advisor for my Master study.

Besides my advisor, I would like to thank my co-advisor and the rest of thesis committee: Assist Prof. Engin Karabudak and Assoc. Prof. Dr. Ali Çağır, Assoc. Prof. Volkan Çeçen, Dr. for accepting to be in my jury, Prof. Dr. Mehtap Emirdağ Eanes, Asst. Prof. Dr. Ümit Hakan Yıldız, Colin McMillen, and Dr. Subrayal Reddy for their collaborated work and also thanks all for their insightful comments, feedback and encouragements for this thesis.

I am as well thankful to the specialists at IZTECH-Center of Materials Research for the SEM analysis.

I also thank to the members of Demir Research Group for their supports during this research. A special thanks to faculty members of Materials Science and Engineering and research assistants of Chemistry Department for sharing their knowledge.

I owe very special thanks to Dr. Onur Parlak for being my brother and his guidance, support, encourage.

Last but not the least; I would like to thank my lovely family: my parents and my sisters for supporting me spiritually throughout writing this thesis and my life in general. This thesis is dedicated to them who have given me their unconditional support, both financially and emotionally throughout my degree.

ABSTRACT

INTEGRATION OF RED & BLUE TL MATERIALS TO DIFFERENT POLYMER END-USE

Triboluminescence (TL) is known as the emission of light upon the application of any mechanical force. In this master thesis, two organometallic-based TL crystals, which are EuD_4TEA and $Cu(NCS)(py)_2(PPh_3)$ were obtained and they were integrated in the transparent polymers: poly (methylmetacrylate) (PMMA), poly (styrene) (PS), poly (urethane) (PU) and polyvinylidene fluoride (PVDF) for different end-use. In the development of composites, two different processes were carried out: i) embedding (or blending) and ii) surface impregnation. The different end-use polymers were used as transparent polymer film, electrospun nanofibers, and nanobeads. TL performance of composites were investigated by using drop tower system which was specficically designed for this research. Atomic force microscopy (AFM), scanning electron microscopy (SEM) were used to characterize the topographic and morphologic properties of both polymers and composites. Additionally, fluorescence microscopy helped to understand the signal of emitted light by composites. Lastly, piezoelectric properties of composite materials were invetigated by oscilloscope. According to results, type of process, particle size of crystal, surface property and form of host material (polymer), the concentration of crystalline particles in composites were determined as the main parameters and the results were estimated with respect to these parameters. PU-based composite film and fiber show better stability towards mechnical stress rather than PMMA, PS, and PVDF due to the roughness surface of thin-film surface for film-based composites, smallest wickerwork formation of electrospun mats for fiber-based composite, and the chemical affinity of PU with TL crystals.

ÖZET

TL ÖZELLİĞE SAHİP KIRMIZI VE MAVİ KRİSTALİN FARKLI POLİMER FORMLARINA İŞLENMESİ

Tribolüminesans (TL) olarak bilinen kristal yapılar mekanik kuvvet altında ışık emisyonu yapma özelliğine sahiptirler. Bu yüksek lisans tezinde, organik ve metal yapıları bir arada bulunduran iki TL kristal elde edilmiş ve bu parçacıklar PMMA (poli metil metakrilat), PS (poli sitren), PU (poli üretan) ve PVDF (poli vinil florür) transparan özellikteki polimerler kullanılarak ince-katmanlı film, elektrospun fiber ve nano boyutundaki tanecikler elde edilen matrisler ile entegrasyona tabii tutulmuştur. Kompozit malzemelerin elde edilmesi için iki farklı deneysel metot geliştirilmiştir: i) yükleme işlemi ve ii) yüzeye depolama işlemi. Kompozit malzemelerin TL performansları bu tez için özel tasarlanan atış kule sistemi ile analiz edilmiştir. Bunun yanı sıra, atomik kuvvet mikroskobu (AFM), taramalı elektron mikroskobu (SEM) polimerlerin ve kompozit malzemelerin topografik ve morfolojik özellklerini değerlendirmek için kullanılmıştır. Ayrıca, flüoresans mikroskobu kullanılarak kompozit malzemelerin emisyon sırasındaki renk sinyalleri belirlenmiştir. Son olarak piezoelectrik özellikleri osiloskop kullanılarak tamamlanmıştır. Tüm bu cihazlardan elde edilen sonuçlar değerlendirildiğinde, deneysel prosedür, kristal parçacıkların boyutları, polimer malzemenin formu ve yüzey özelliği, kullanılan kristallerin kompozit içindeki miktarı bu çalışmada temel parametreler olarak belirlenmiştir. PU esaslı elde edilen film ve fiber kompozitler PMMA, PS, ve PVDF esaslı kompozitlerden daha iyi sonuç göstermiştir. Bunun nedeni olarak, film esaslı kompozitler için ince katmanlı PU filmin daha engebeli bir yüzey olması; fiber esaslı kompozitler için elektrospun PU fiberin daha küçük yapılardan oluşması, tüm bunlara ek olarak PU'nın kimyasal olarak TL özellikteki iki kristalle kimyasal etkileşim oluşturulması gösterilebilir.

Dedicated to my parents…

TABLE OF CONTENTS

LIST OF FIGURES

Figure **Page**

LIST OF TABLES

CHAPTER 1

INTRODUCTION

1.1. Motivation

Light is the electromagnetic radiation causing by the emission of absorbed atom in different ranges.(O'Hara, Engelson, and St Peter 2005) Atoms and molecules emit light at specific energies; therefore, the relaxation of each specie give characteristic color. Light emission has two mechanisms: spontaneous and stimulated. Spontaneous emission occurs by the help of flames or discharge lamps. Stimulated emission takes place by the perturbing of photon. Figure 1.1. shows that there are various types of light emission.(Olawale et al. 2011) The classification of light emission can be divided by the process of heating or not, firstly. If the heat is the outcome of light emission, this type is called incandescence emission. This is special term of thermal radiation.(Acikgoz and Gnutek 2014) The response of light emission without heating is called as luminescence. This type is known as cold body radiation that is caused by chemical reaction, mechanical forces onto crystal, electrical energy releasing, movement of atomic disturbing. If mechanical forces are not dominant for light emission, there are two types of emission response which are excited with or without light. If the excitation source is the light, fluorescence and phosphorescence come to the fore. Fluorescence is known as the immediate emission provided by absorbed light or electromagnetic radiation (EMR). Phosphorescence has the same conditions for fluorescence; however, it takes longer time to re-emit the radiation. Chemiluminescence and bioluminescence are related to light emission without excitation by light.(Yu et al. 2009, Welsh et al. 2009) These emissions occurs as the result of chemical reaction. Bioluminescence is the type of chemiluminescence which is produced by a living organism.

Triboluminescence (TL) is known as the emission of light upon an appiled of any mechanical force. This phenomenon comes from mechanoluminescence (ML). This classification defined as three types of excitation for tribo-based processes: electrically, chemically, and thermally. Electrically induced tribo materials cause triboelectric field during friction of two dissimilar materials. When these two dissimilar materials exposed to rubbing, the chemical reaction takes a place to produce chemically induced tribo

ability; however, when the mechanical force provides any heat production of two materials, it is called as thermally induced tribo material. These all concepts are mainly based on that the most established definition of triboluminescence is that the breakage of a crystalline structure during mechanical force that causes charge separation; therefore, energy releases as light emission.

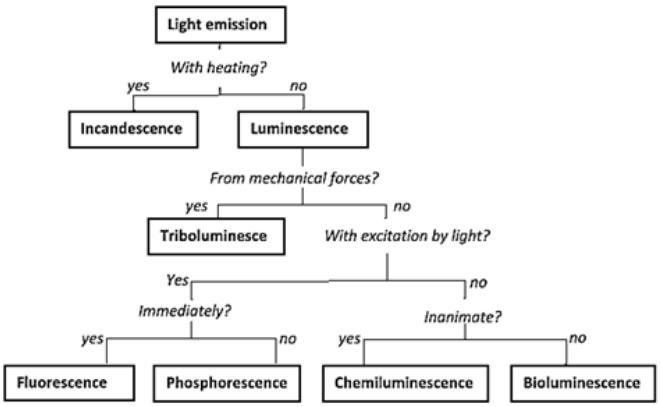

Figure 1.1. The schematic illustration for the classification of light emissions

Considering the concept of stress-sensitive behaviour of TL materials, the current problem is to immediate detection when the materials are exposed to damage. In order to get over this issue, composite materials can help to utilize the application of TL sensors. Furthermore, composite materials including by TL molecules allow to monitor the mechanically failure or impacts in the structural form. Integration of EuD_4TEA and $Cu(NCS)(py)_2(PPh_3)$ TL materials into various polymers, poly(methyl methacrylate), poly(styrene), and poly(urethane) by two different experimental process open a way to develop smart sensors and generate new mechanosensing technology. Using a specilized drop-tower system, the triboluminescent properties of fabricated TL/transparent polymer composite films can be characterized in terms of light yield and decay times.

1.2. Structure and Scope of the Thesis

The first chapter of thesis gives an introduction and the purpose of the research. In *chapter 2,* a comprehensive literature review is done. This part includes detailed information about triboluminescent materials such as EuD_4TEA, $Cu(NCS)(py)_2(PPh_3)$, and triboluminescent polymers. Experimental part is given in *chapter 3,* and in *chapter 4* results will be given with their discussion. In *chapter 5,* concluding remarks will be explained.

CHAPTER 2

LITERATURE REVIEW

2.1. Triboluminescence

TL is the emission of cold light. The principle strategy for the produced TL is based on the light emission by mechanical forces such as crushing, fracturing, smashing and grinding.(Jha and Chandra 2014, Fontenot, Hollerman, et al. 2012) When the crystals are subjected to applied forces, the physical deformation occurs initially. The change in physical conformation leads to produce charge separation. Both positively and negatively separated clouds cause electrical field. When the electrical field produced, the electron delocalization between separated charges behaves like piezoelectric materials. Mechanically produced charge separation ends up with triboluminescence emission, when the mechanical forces taken out of the crystal. Thus, TL emission occurs the occurence of this mechanism consequently. When the mechanical forces is to end, the charge delocalization results as decay; therefore, light emission is quenched.

The circle for the mechanism of TL emission has been explained eventhough there is no established theory, yet. The origin of TL based materials is directly related to the symmetry property of crystal structure. Most of the crystals, which show TL property has non-centrosymmetric conformation. This type of formation is enough to take response TL emission. However, some materials do not have desired assymmetry for TL emission. For this case, the addition of dopant materials or impurities help to provide the needed space between two crystal for the production of TL emission. Additionally, the crystals which have lack of stacking formation have higher tendency to emit high percentage TL due to the longer travel pathway for electron delocalization.

2.2. Examples for TL materials

TL property can be observed in both inorganic and organic crystals ordering of symmtery in unit cell. Sugar, saccharin, phthalic anhydride, and zinc sulfide are known as self-TL materials.

For instance, sugar has packed crystalline structure. (Chandra 1976) The most commonly used sugar form is known as sucrose; however, it is the form of stucking two

simple sugar molecules, which are fructose and glucose. The dry sugar has the crystalline form of cubelike shapes. They have orderly arrangement with packed assay. When sugar crystals are smashed, they show blue triboluminescence emission. The mechanism of triboluminescence includes electrical field generation, charge separation, and release energy to get reunite as TL emission.

In addition to organic crystals, inorganic and organo-metallic based crystals show TL emission. They are ZnS:Mn (Mei et al. 2001), $SrAl_2O_4$:Eu, Ce, Ce-Ho, $SrMgAl_6O_{11}$:Eu, $SrCaMgSi_2O_7$:Eu, $SrBaMgSi_2O_7$:Eu, $Sr_2MgSi_2O_7$:Eu, $Ca_2MgSi_2O_7$:Eu,Dy, $CaYAl_3O_7$:Eu, $(Ba,Ca)TiO_3:Pr^{3+}$, $ZnGa_2O_4$:Mn, $MgGa_2O_4$:Mn, $BaAl_2Si_2O_8$:rare earth elements, $Ca_2Al_2SiO_7$:Ce, ZrO_2:Ti, (Chandra and Chandra 2012, Akiyama, Nishikubo, and Nonaka 2003, Xu et al. 2004, Chandra et al. 2009, Chandra et al. 2011) ZnMnTe, ZnS:Mn,Te (Reddy and Reddy 2002, Sun, Li, and Tay 2003) and MgF_2:Mn, La_2O_2S:Eu, and Y_2O_2S:Eu (Hollerman et al. 2012) have also TL emission. These all materials are classified as mechanoluminescence groups, which is mainly based on dislocation-induced process to obtain TL emission from both physical and chemical deformation.

2.3. Lantanide Based TL Materials

Owing to the growing interest in triboluminescence materials, the synthesis of lanthanide (Nd, Eu, Gd, Tb, Dy, Ho, Er, Tm, and Yb) based TL complexes has been important research area due to excellent ability of lanthanide to emit light with a narrow band, long-lived excited states, and high quantum yield.(Bunzli and Eliseeva 2013, Oliveira et al. 2016, Souza et al. 2016) However, direct excitation does not give luminescent response because of spin forbidden state for $f - f$ transitions of lanthanide.(Biju et al. 2013)

The reason is that Ln^{III} based complexes contain antenna molecules such as aromatic carboxylates, phosphonates and sulfonates, heterocyclic structure and β–diketonates in order to light-harvesting and energy transfering around lanthanide ions.(Eliseeva et al. 2010) Among those e-donating group containing molecules, β–Diketonates come to the fore with more advantages due to the formation of octa coordinate tetrakis or hexa coordinate tris complex.(Teotonio et al. 2008, Eliseeva et al. 2011, Bunzli et al. 2010) This condition is required to negative charged binding formation

by an ancillary ligands, which are mostly known as *N- or O- donor,* to complete chemical structure and gain neutral formation by tuning photophysical properties.(Eliseeva et al. 2010) Moreover, these groups are able to increase the absorbed photon by lanthanide ions; therefore, due to the higher population of absorbed photons, energy transfering through the complex can be enhanced by increasing of the emitting photons by $f - f$ transitions. Therefore, β–Diketonates provides highly emissive, sharp and easily detectable transition state by instrumentally, this structure leads to the improvement on mechanosensing platform.

2.4. Eu(III)-based Compound: EuD_4TEA

In the development of lantanide based triboluminescence, there is a well-known example, europium tetrakis(dibenzoylmethide) triethylammonium compound (EuD_4TEA). It is one of the brighest organo-metallic TL material. EuD_4TEA was synthesized in anhydrous solvent condition according to the synthesis proposed Hurt et. al. in 1966. Eu(III) derived TL material has an e-donating group, which is 1,3-Diphenyl-1,3-propanedione (DBM) as β–diketonate form, and e-withdrawing group, which is triethylamine (TEA) as negatively charged coordination completing group. This kind of tetra-bidentate complexes exhibit eight-coordinate rare-earth propanedionate structural form with square-antiprism geometry.(Bunzli and Eliseeva 2013)

This non-centrosymmetric compound, EuD_4TEA, has a triboluminescence property due to having that much disorderance on centrosymmetry and packed crystal stacking. In terms of Ln^{III} tetrakis(β–diketonate) complexes, Eu(III) based complex presents higher quantum yield and lifetime. For photoluminescent characterization of the TL material, the triplet state energies of these ancillary ligands, which are DBM and TEA, display bright red luminescence due to characteristic transition from $^5D_0$ to ^7F_J (J = 0-4). EuD_4TEA crystalline material in organic solvent shows the highest photoluminescence emission transition from $^5D_0$ to $^7F_2$, which is centered around 614.0 nm.(Khalil et al. 2004) In the synthesis of Eu(III) based triboluminescence material, the europium salt form is directly effected onto triboluminescence emission. For instance, $EuCl_3$ allows completing TL crystal structure for EuD_4TEA; however, dissolved chlorine as residue behaves as quencher anionic form around the compound. Therefore, EuD_4TEA, which was synthesized by $Eu(NO_3)_3$, exhibits 82% TL emission than $EuCl_3$ based compound.(Fontenot et al. 2011) The study on synthesis of EuD_4TEA by different

solvents can open a way to understand how the solvent type is effective on crystal size, triboluminescence property, quantum yield and decay time.(Fontenot, Bhat, Hollerman, Aggarwal, et al. 2012) In terms of triboluminescence emission, the compounds, which were synthesized by cyclic group based and acidic solvents, have no TL response. On the other hand, carbonyl group containing, alcoholic, and some miscellaneous (chloroform, acetonitrile, ethyl ether) solvents showed TL response. Among those solvents like acetone, ethyl acetate, ethyl alcohol, 1-butanol, etc.; acetone (lab grade) derivative EuD_4TEA has the larger crystal size with the highest photoluminescence emission. In contrast, the EuD_4TEA, which was synthesized by chloroform, has the smallest crystal size with the lowest photoluminescence emission. It was understood that there is a proportionally correleation between grain size of particles and triboluminescence emission.(Fontenot, Bhat, Hollerman, Aggarwal, et al. 2012)

Moreover, lanthanide series were all treated by dibenzoylmethane and triethylammonium in order to synthesize lanthanide-based triboluminescence material and those different materials were compared in terms of triboluminescence emission.(Fontenot, Hollerman, Bhat, Allison, et al. 2013) The spectral differentiation on TL emission among $Ln^{III}D_4TEA$ compounds was reported as directed to material dependent structural configuration, discharge varying of gap into molecule, and empty orbital orientation for emission transitions. Photoluminescence colours of each luminescent material can be ordered for Pr, Ho, La, Ce as colorless; Dy, Nd, Tb, Yb as green; Er, Sm, Gd as red; on the other hand, Eu shows bright red emission colour. Among those materials, triboluminescent emission of Sm, Gd, Nd, Pr, Tb, Yb, and Eu were compared. As a result, EuD_4TEA has the brighest triboluminescent emission, the longest decay time, and the highest quantum yield. This result is related to that wide absorption interval of Eu(III) derivative compound can allow to be donated much more electron for emission states.

In the comparison of triboluminescence emissions of inorganic, organic, organo-metallic and lanthanide based luminescent materials, there is a recent study to understand the triboluminescent concept of materials and to improve TL-based mechano-sensor systems. Triboluminescence ability of materials was evaluated according to these three properties: chemical composition, crystal size as physical property and the effect of dopant material. ZnS:Mn, ZnS:Mn,X (X:Cu, Pb) , La_2O_2:Eu, Y_2O_2S:Eu, EuD_4TEA and 27 luminescent material like previous ones were analyzed by drop-tower system for

triboluminescence emission measurement.(Hollerman et al. 2012) It was reported Dimethyl methylphosphonate doped EuD_4TEA showed the highest TL emission, which was two times higher than undoped EuD_4TEA and three times more TL capacity than Mn doped ZnS material.

From this way, in order to investigate dopant effect on EuD_4TEA, piperine (lab grade), triethylphosphine sulfide(TEPS), Dimethyl methylphosphonate(DMMP), caffeine(Fontenot, Hollerman, et al. 2012) and uranium(Fontenot, Hollerman, Bhat, and Aggarwal 2013) were doped into EuD_4TEA. Among them four different dopant materials showed different increase on TL percentage like that the triboluminescence yield of EuD_4TEA for piperine (lab grade), caffeine, uranium and DMMP were 20%, 50%, 100%, and 200%, respectively. approximately. Additionally, multivitamin doped EuD_4TEA shows different TL emission. (Fontenot, Bhat, Hollerman, and Aggarwal 2012)

2.5. Cu(I)-based Compound: $Cu(NCS)(py)_2(PPh_3)$

One of the newest example for TL materials, inorganic compound containing copper, pyridine and triphenylphosphine. The synthesis procedure for this compound has a clear process and the system allows to obtain great crystalline formation as triangular prism. In a typical synthesis, molecular compound with the four-coordinate Cu(I) center in a tetrahedral for with composed of N-bonded thiocyanate, two pyridine, and one triphenylphosphine. This crystal form is called monoclinic structural morphology. It has lack of symmetry by the packing of molecules along x-axis. When any mechanical force is applied, the triboluminescent emission might be originated from the breaking of Cu-NCS bonds. The breaking of inorganic form causes charge separation as positively (Cu-cations) and negatively (-NCS anions). This charge separation cause electrical field; therefore, detected triboluminescence emission is the resultant of this noncentrosymmetrical change into molecular level.(Marchetti et al. 2012)

2.6. Association of TL materials with polymers

Polymers are known as macromolecules, which are made of many repeating units are called monomer. The repating unit of polymer are mostly made of carbon and hydrogen; however, oxygen, nitrogen, sulfur, fluorine, chlorine, phosphorus and etc. can be linked with respect to polymerization process depending on desired chemical construction.

In recent years, smart polymer composite materials exhibit great optical properties for mechano-sensing. Polymers are good candidate and multi-functional materials for solid membrane to use them in TL applications. Polymers come to the fore solid support to manage TL material for the designing of mechanosensing platform. Most of the luminescent applications, polymer-particle composite can exhibit developed properties and utilized funtionalities for generating new concept materials. In terms of triboluminescence, how mechanical forces (stress) are transferred on a polymeric system instead of pristine TL crystals can open a way to understand the behaviour of impact-induced composites. Therefore, improvement on smart materials for this methodology have a potential to investigate molecular-level composition, optical and mechanical properties. Additionally, the effects of shape, size of particles and different process to obtain composite films might be demonstrated. Fabrication of TL/polymer composites exhibits the determination of light variation, mechanically behaviour, resistivity, and photophysical properties of materials. Moreover, polymers can be obtained as transparent films when moderate substrate is used and annealing process is carried out. The modification of transparent polymer film by TL crystal provide to eliminate any transmission and scattering of emitted light. (Pu et al. 2015, Jin et al. 2013, Raja et al. 2013)

Integration of TL materials into polymers has been emerged in a variety of stress based platform and the development of stress probes. The main point for these concepts rely on loaded mechanical force and the response of composite materials in the during of stress-strain behaviour. These both aspects provide to understand tensile mechanical properties of composites. Mainly, triboluminescent based composite materials allow to develop mechanoluminescence materials. Therefore, highly effective materials may open a way to specify a failure, evaluate stress concentration, compute failure onto composite and characterise fracture mechanism. These all utilize having potential for simple, real-time monitoring of both magnitude and damage from finger pressure to higher level onto the host material. (Chandra, Chandra, and Jha 2015, Olawale et al. 2011, Fontenot et al. 2014)

The studies on incorparation of inorganic or organo-metallic based TL materials into polymer matrices provide to understand selective adsorption of crystal particle by surface, TL emission transfer on the crystals from polymer media and the effect of experimental process on dispersion of particles in polymers.(Meuer and Zentel 2008)

Furthermore, the designing of TL/polymer composite materials is required surface functionalization on polymer form if the covalent bonded is needed to success TL emission. (Asefa et al. 2002) In terms of micro-damage sensing system, using fiber-reinforced-composites has come to the fore to determine failure loading cycle on composite materials.(Dickens et al. 2015) In the photonic applications of lanthanide based luminescent materials, most of triboluminescent materials are included by the conjugation of e-donating group, hexafluoroacetylacetonate (hfa).(Hasegawa and Nakanishi 2015) This ligand allows to synthesize the triboluminescence lanthanide coordination polymers. The coordination of self-TL polymers shows great TL emission with higher mechanical properties.

2.7. Piezoelectricity of PVDF

Piezoelectric substance is known as the materials that produce an electric charge after the application of a mechanical stress. When any electric field is carried out, a mechanical deformation forms in the material. The specific distribution of electric changes in the unit cell of a crystal is called as piezoelectric effect. This produced electricity and the voltage of these electrical charges are proportional to the stress which is applied.(Gusarov et al. 2016)

The first piezoelectric effect was observed in 1880. The most common natural piezoelectric material is quartz. However there are some biological materials which are tendon, silk, dentin and DNA exhibit piezoelectric property. Langasite, lithium niobate, lithium tantalate and barium titanate, lead zirconate titanate are known as synthetic crystals and ceramics, respectively.(Ahn and Son 2016) Unlike ceramics and crystals, polymers shows piezoelectricity. Specifically, PVDF (polyvinylidene fluoride) is known as the semi-crystalline piezoelectric material with some advantageous such as producing higher amount of electrical charge rather than quartz. The crystalline phase of interest for PVDF ferroelectricity is the polar β phase.(Seminara et al. 2011)

PVDF polymer offers great advantages over ceramic such as they are flexible and therefore can be formed easily. Additionally, PVDF is chemically inert, tough, creep, resistant, and has good stability when it exposed to sunlight.(Jain et al. 2015)

There are some studies on the piezoelectric properties of PVFD-based composites. For instance, PVDF-trifluoroethylene mixing silver nano-fillers exhibits an improvement

of the β phase crystallization and the enhancement of piezoelectric performance of PVDF polymer.(Chen et al. 2016) Another study is the composition of nano-ZnO/PVDF composite films to make them useful in energy harvesting application.(Bhunia et al. 2016) In terms of advanced studies, flexible plasmonic nanogenerator are classified as new class when the plasmonic properties of graphne-silver nanocomposite were combined with the piezoelectric properties of PVDF.(Sinha et al. 2016)

CHAPTER 3

EXPERIMENTAL SECTION

3.1. Materials and Methods

Europium(III) nitrate pentahydrate (99.9% trace metals basis), 1,3-Diphenyl-1,3-propanedione (DBM, 98%), triethylamine (TEA, ≥ 99%), copper (I) thiocyanate (99%), triphenylphosphine (99%), pyridine (anhydrous, 99.8%), alginic acid sodium salt (powder), calcium chloride dihydrate (ACS Reagent, ≥ 99%), styrene (99%), Divinylbenzene (DVB, technical grade, 55%), Benzoyl peroxide (BPO, 75%, remainder water), poly (methylmethacrylate) (PMMA) (~350 kDa), poly(styrene) (PS) (~350 kDa), poly(urethane) (PU-SKU:81367), poly(vinyl alcohol) (30 kDa – 70 kDa) and ethanol (≥99.8%) were purchased from Sigma Aldrich (St. Louis, MO, USA). All other reagents and solvents are avaiable at analytical grade and were purified before use. Scanning Electron Microscopy (SEM), FEI Quanta 250 Feg (Oregon, USA) was used to characterize surface morphology. Fluorescence images were recorded due to Fluorescence Microscopy Olympus IX2-ILL100 (New Jersey, USA). Photoluminescence emission spectra were recorded by Varian Cary Fluorescence Spectrophotometer (Palo Alto, USA). A home-made drop tower system was designed and prepared consisting of USB2000+ Preconfigured 200-850 nm UV-Vis Spectrophotometer and fiber optic cable (Ocean Optics, Florida, USA). Piezoelectricity measurements were done by using Digital Storage Oscilloscope GDS-1000-U Series (New Taipei City, Taiwan).

3.2. Synthesis of EuD_4TEA

The synthesis method of EuD_4TEA in Figure 3.1, which was published in the past, was modified and started with 4 mmol of dibenzoylmethane was dissolved in 50 mL of anhydrous ethyl alcohol at 100^oC. After completed dissolution, 13 mmol of triethylamine was added into the solution. On the other hand, 4 mmol of Europium(III) Nitrate Pentahydrate was dissolved in 25 mL of anhydrous warm ethyl alcohol and the solution was sonicated for 2 min by ultrasonic bath. Lastly, Eu(III) salt solution was added into the main container, which was included DBM and TEA. The reaction was stirred and heated up to 200^oC degree in 1 h under controlled manner. When the whole solution

became clear, the heating process was finished. It was firstly allowed to cool down the solution at room temperature and then it was placed into +4^{o}C degree to kept under darkness overnight. The formed crystal particles were filtered by using vacuum filtration system and they were air dried.(Fontenot, Hollerman, et al. 2012)

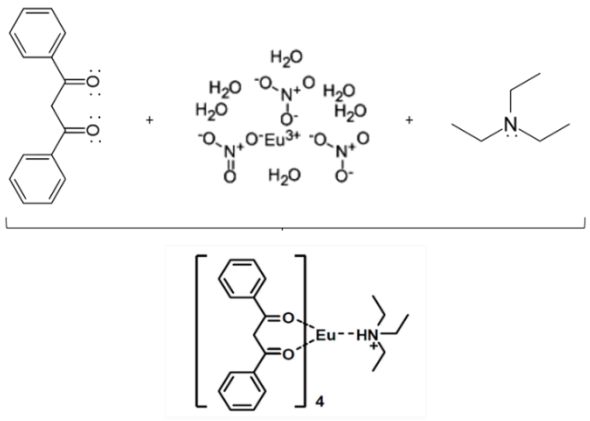

Figure 3.1: The synthesis schematic for EuD_4TEA compound with chemical structure

3.3. Synthesis of $Cu(NCS)(py)_2(PPh_3)$

The synthesis process for Cu(I) based triboluminescent material in Figure 3.2. started to put all components, which are 1.00 mmol of CuNCS and 1.00 mmol of PPh_3, into 5 ml of pyridine. The solution was stirred by heating up to 70^{o}C. The reaction was allowed to mixed for 3 h. When the reaction was completed, the warm blue colored solution was obtained. The solution was left for slow cooling, overnight. At the end of cooling process, pale-yellow crystals were obtained by vacumm filtration and rinsed by toluene.(Marchetti et al. 2012)

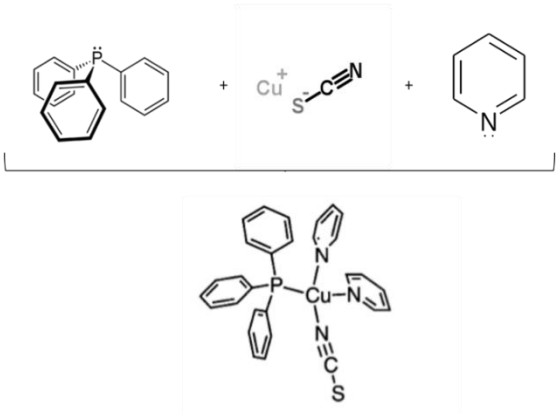

Figure 3.2. The synthesis schematic for $Cu(NCS)(py)_2(PPh_3)$ compound with chemical structure

3.4. Preparation of TL/transparent polymer films

In order to obtain TL/polymer composite films, two different process were carried out: i) embedding and ii) surface imprenation (Figure 3.3.). Three different transparent polymers were employed: polymethyl metacrylate (PMMA), polystyrene (PS) and polyurethane (PU). The weight concentration of each polymer solution was 15%. The concentration of TL material in composite was fixed at 2.5% (g/mL). *In embedding (or blending) procedure*, each polymer solution was prepared as follows. After dissolving, determined mass dye material was added into solution and allowed to mix together. When the homogeneous dye polymer solution was obtained, the solution was casted onto glass surface. In order to evaporate solvent, annealing process was carried out under 100^{o}C for 2 h. Eventually, transparent dyed polymeric film was obtained. *In surface impregnation process*, the prepared polymer solution was processed by film casting and then annealing process as the same condition with embedding process. Then, transparent polymer film was cut on the order of a cm. The dye particles were dispersed into 10 mL of distilled water by using ultrasonic bath. The each cutten film was put into dispersed dye solution and treated one day by shaking to ensure that the surface of polymer film was impregnated by TL material.

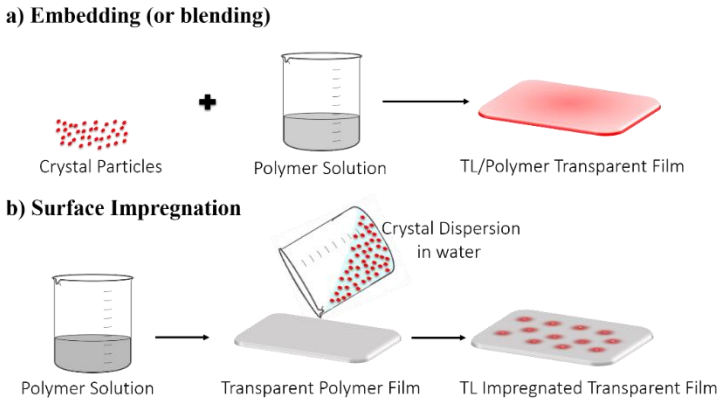

Figure 3.3. The illustration of two different process: i) embedding (a) and surface impregnation (b) for the preparation of composites

In order to investigate the effect of dye percentage into polymer, polyurethane composite films were prepared by different [EuD_4TEA] in composites by embedding method. The concentration of polymer was fixed at 15% wt. and [EuD_4TEA] is varied from 10 to 99 percentage by mass. The embedding process was carried out under the same condition.

3.5. Preparation of TL/electrospun fibers

Electrospinning is as an efficient method that has been well-established and scalable technique for the fabrication of continuous fibers with the range of different diameters down to a few nanometers from polymer solution.(Demir et al. 2002, Demir et al. 2009)

The instrument has three main components in Figure 3.4 which are: i) a capillary tube with a pipette or neddle of small diameter, ii) a high voltage supplier, and iii) a grounded metal collector panel. In order to obtain fibers, firstly, the solution is pumped through needle. During this process, the high voltage supplier is used to generate an electrically charged jet of polymer out of the tube. The nozzle of the needle behaves as an electrode and it feeds to created 100-500 kV m^{1-} applied electric field. The solution starts to evaporate and solidify when it is transported by the electric field. Furthermore, the interdependent web or reticular forms is spread out on the collecting screen. (Mayuri and Ramesh 2016, Lawson et al. 2016, Rieger, Birch, and Schiffman 2016) Additionally, the principle mechanism for electrospinning instrument is based on four parameters: i) viscosity of solution, ii) solvent of the solution, iii) applied voltage, and iv) pumping rate.

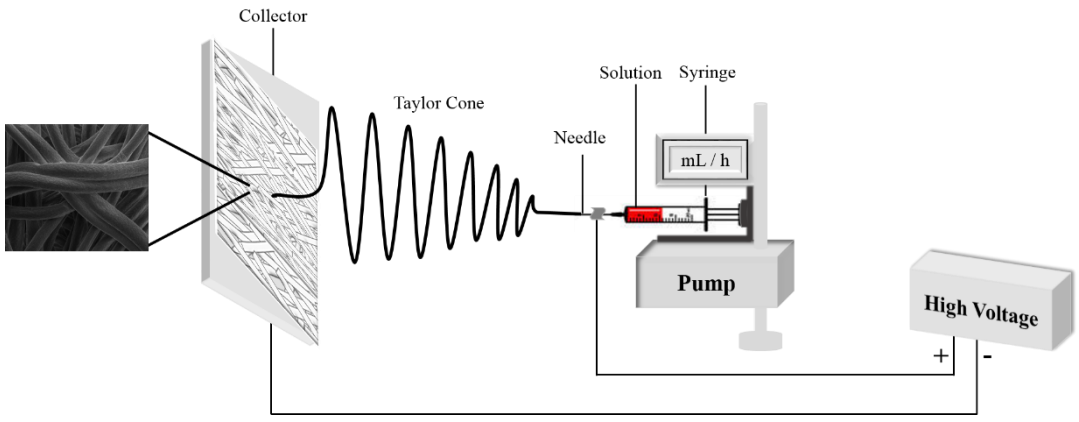

Figure 3.4. Schematic representation of electrospinning instrument

In order to obtain TL/electrospun fiber composites, two different process were carried out: i) embedding and ii) surface impregnation. The same polymer, which are PMMA, PS and PU like polymer films, were employed. The concentration of each prepared polymer solution was fixed at 15 wt. The concentration of TL material was fixed

at 2.5%. *In embedding (or blending) procedure*, each polymer solution was prepared at the beginning. Then the determined mass TL material was added into polymer solution and allowed to mix together. When the homogeneous dye polymer solution was obtained, each polymer solution was taken into the syringe to process TL embedded polymer fibers by electrospinning instrument. The condition of electrospinning was fixed 18 kV., 4 mL/h., and 50% for applied voltage, pumping rate and humidity of air, respectively. In surface impregnation process, the fiber mats were prepared by cut on the order of a cm (Figure 3.5.). The round shaped fiber mats were placed into the syringe. Each membrane was treated by 2.5% of dispersed crystals solution for one time. Finally, the surface impregnated fiber mats were dried in air.

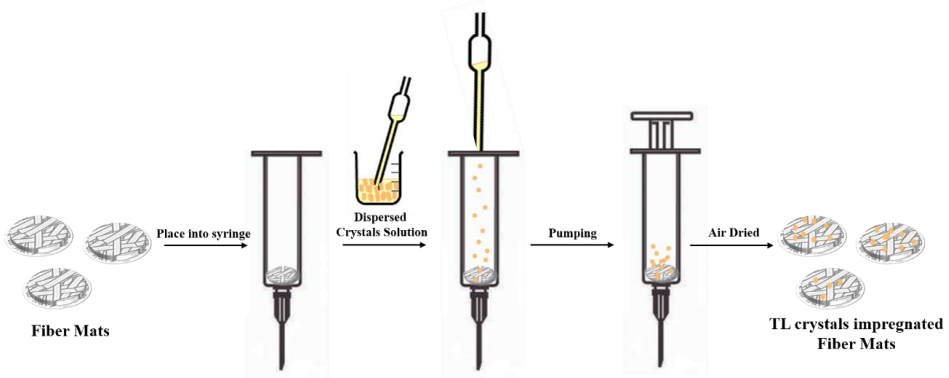

Figure 3.5. The illustration of surface impregnation process for the preparation of TL/electrospun fiber composites.

3.6. Synthesis of EuD_4TEA /PS Nano Beads

In order to synthesize PS-based beads, the suspension polymerization technique, which is known as solid-phase organic synthesis, was used (Figure 3.6). The synthesis was started to prepare monomer/initiator medium. Styrene were used as monomer. Benzoylperoxide (BPO) was used as initiator. In order to prepare the main solution, 0.1 gram of BPO was added into 10 ml of monomer solution. After that the dissolution of initiator into monomer, 1 mL of 1,4-Divinylbenzene (DVB) was syringed into each main solution. DVB was used as a reactive monomer to form cross-linked co-polymer network. Lastly, 100 mg. of EuD_4TEA crystal particles were added into the solution. Separately,100 mg. of poly(vinyl alcohol) (M_w: 30 – 70 kg/mole) was dissolved in 80 mL of warm distilled water. PVA was an effective material to increase the hydrophilicity of polymer-DVB resin because of low swellability in polar media of bead composite. When

the PVA was completely dissolved, the solution container was placed into oil bath. The heat was regulated at 90°C and it was under controlled by thermometer during the whole polymerization process. Then, the mixture was poured into PVA solution. The flask was closed by using rubber stopper. A sharp needle was inserted into the container by penetrating the rubber. In order to keep the polymerization conditions constant, nitrogen gas (N_2) was let to flow at moderate rate into the container. N_2 gas behaves as a prohibitive agent to protect the intake of oxygen and moisture from surrounding. The formation of polymer beads took two hours. When the polymerization was completed, the solution was poured into large amount of methanol to separate the polymer. The wholesolution was filtered and dried under vacuum. The same reaction was repeated to synthesize PS NPs without crystals.

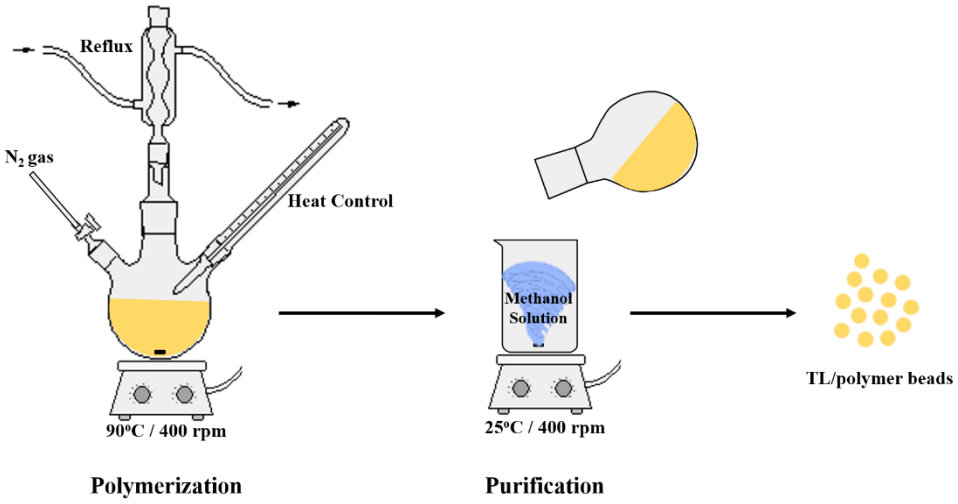

Figure 3.6. The synthesis mechanism for EuD_4TEA/PS nanobead composites

3.7. Drop Tower System

The triboluminescence emission of TL and TL/polymer composite materials were measured by using drop tower system. The system was specifically designed for the TL measurement and shown in Figure 3.7. The material was placed into sample holder, which is on the black box. A 50 gram steel ball with a diameter of 1 cm is positioned on a pull pin at a set distance 20 of inches (50 cm) above the material. When the pin is pulled, the ball falls and hits onto the material leading to produce TL. A fiber optic cable is placed directly into the small hole inside the black box to catch and transfer upon impact radiation through the spectrophotometer. By using custom Labview program, the spectral change was obtained by quick view fluorescence mode as the graph of triboluminescence

emission with respect to wavelength. In order to calculate applied force on composites, the drop-tower system was taken into consideration as the motion of free fall object. The free fall balling has two components: i) distance and ii) velocity shown in equation 1 and 2, respectively. Impact force from falling object has two energies, which are potential and kinetic. The system has potential energy (ε_p); however, the kinetic energy (ε_k) is zero before free falling.(Figure 3.8) After loaded impact on composite materials, the whole potential energy is converted and used to generate kinetic energy. Therefore, when the ball hits onto composite, the system reachs up to maximum kinetic energy; however, the whole potential energy is spent by the system. Furtermore, the total change in the kinetic energy of an object results as the total work done on the composite. The average impact force was calculated by using this principle of work-energy.

Equation 1: $h = \frac{1}{2} gt^2$

Equation 2: $v = g.t$ $(g = 9.80\ m/s^2)$

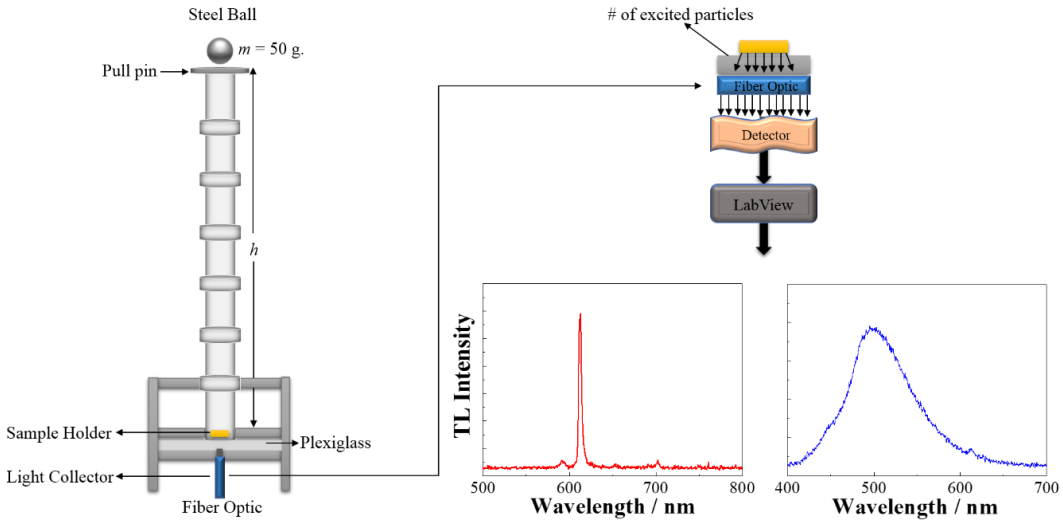

Figure 3.7. Schematic diagram of drop tower system, which was specifically designed for composite films

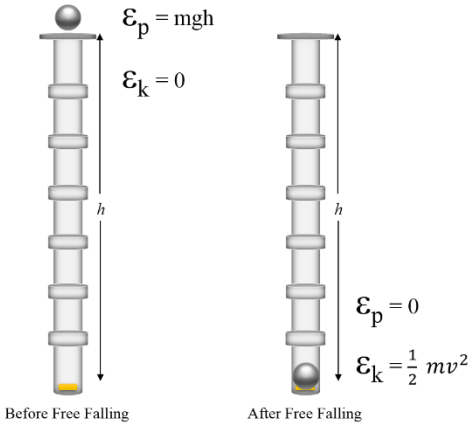

Figure 3.8. The energy substitution process by the motion of free falling objects

3.8. Piezoelectric Voltage Measurement and Set-up

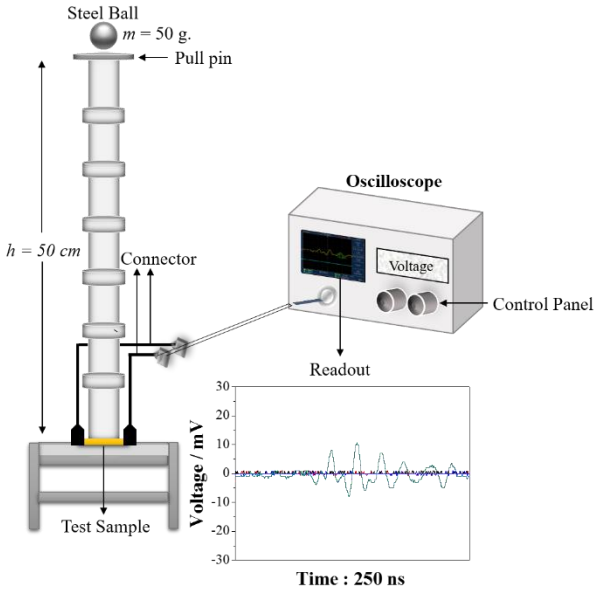

Figure 3.9. The schematic illustration of set-up for piezoelectric voltage measurement

The schematic illustration of the set-up for piezoelectricity measurement is given in Figure 3.9. Drop tower mechanism is combined with oscilloscope for the measurement of amount of produced piezoelectric voltage. The composite film is placed on the smooth surface. Two conductive connectors are fixed to the end-points of composite film. Two ends are connected the probe of the oscilloscope. The probe is a sharp tip and it is a point for main circuit. When the probe carry a signal to the scope, it builts a readable votage on the control panel. For the voltage characterization, the amplitude is a measure of the

magnidute of produced signal. In other way, this is known as peak-to-peak amplitude which measure the absoluted difference between a high and low voltage point of a signal. The peak amplitude should be fixed 0V as a background and the measurement voltage interval was fixed between -50 mV to +50 mV. Additionally, the measurement time is fixed as 250 nanoseconds.

In order to create mechanical stress, the same methodology in triboluminescence characterization of composite is used. The metal ball (50 gram) is positioned at 50 cm higher than test sample. When the pin is pulled and the ball hits the material, the produced piezoelectric voltage is recorded by read-out of oscilloscope. By using the trigger system of oscilloscope, the signal is stabilized and saved.

CHAPTER 4

RESULTS and DISCUSSIONS

4.1. Characterization of TL Crystals

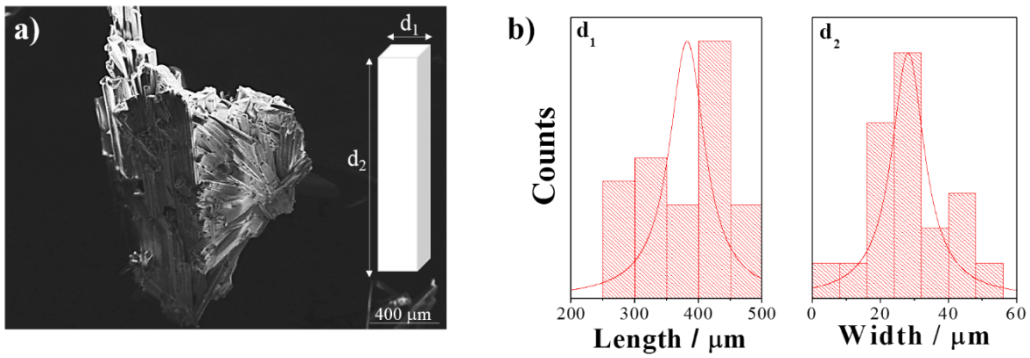

Figure 4.1. SEM image (a) and Particle Size Distribution (b) of EuD_4TEA

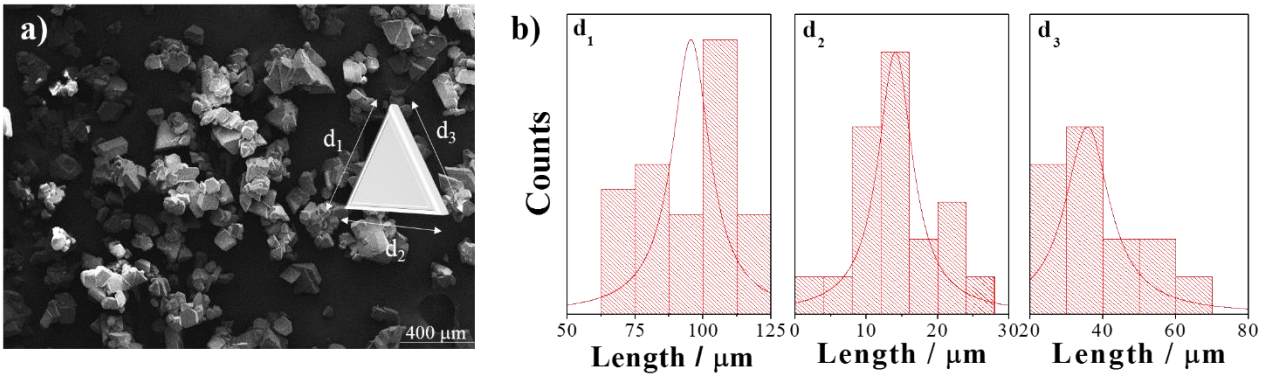

Figure 4.2. SEM image (a) and Particle Size Distribution (b) of $Cu(NCS)(py)_2(PPh_3)$

In order to determine the morphologies of both TL crystal particles, the images of scanning electron microscopy (SEM) were obtained. They are shown in Fig. 4.1.a and 4.2.a. For Eu(III) derivative compound, the crystals have prizmatic shape. This morphology is compatible with the classification as square antiprizm model, which is defined in literature. For Cu(I) compound, most of the crystal particles have triangular prizm structure and it is compatible with the literature. Moreover, for both cases, each single crystal is situated in a simultaneously repeating or periodic array to become stacked form. The whole block is formed in a repetitive three-dimensional pattern, in which each single crystal is physically bonded to its nearest-neighbor crystal. In terms of impact-

induced composite, triboluminescence emission of materials is directly related to the size of crystal particles. The size distributions of both synthesized crystals are obtained from SEM images to measure both height and diameter size by using ImageJ.

The size distribution of EuD_4TEA crystal was shown in Fig. 4.1.b. Both graph have broad distribution and the average size is 350 μm and 30 μm for height *(d_1)* and diameter *(d_2)*, respectively. The size distribution of $Cu(NCS)(py)_2(PPh_3)$ crystal is shown in Fig. 4.2.b It seems that for three length, the average size is changing as 80 μm, 15 μm, and 50 μm for d_1, d_2, and d_3, respectively.

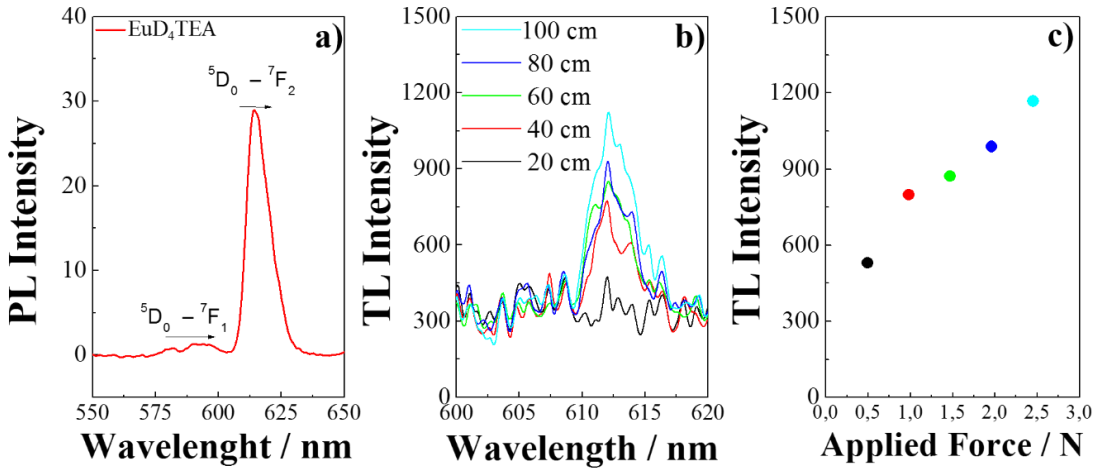

Figure 4.3. Characteriztion panel of the bulk form of EuD_4TEA: PL (a), and TL (b) at different heights and TL emission with respect to applied force (c)

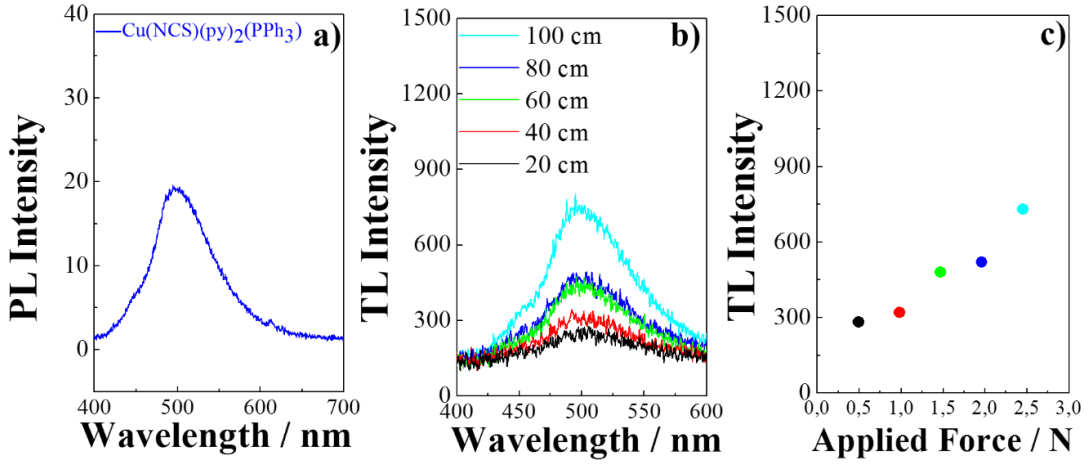

Figure 4.4. Characteriztion panel of the bulk form of $Cu(NCS)(py)_2(PPh_3)$: PL (a), and TL (b) at different heights and TL emission with respect to applied force (c)

In terms of the luminescent properties characterizations for TL materials, the spectral fearutes were shown in Figure 4.3. and 4.4. for Eu(III) and Cu(I) based material, respectively. EuD_4TEA was dissolved into N,N-Dimethylformamide (DMF). Figure 4.3.a exhibits PL spectrum of the dye solution. The graph illustrates a classic transition state for Eu(III) lanthanide based fluorescent material. The main transition from $^5D_0$ levels to the lower $^7F_2$ is centered at 614.0 nm. For Cu(I) based material, blue emission is centered at 496.0 nm for the highest emission (Fig. 4.4.a). Triboluminescent spectra was taken by using drop tower system and each triboluminescence emission of EuD_4TEA and $Cu(NCS)(py)_2(PPh_3)$ was recorded from different heights by using same mass steel ball Figure 4.3.b and 4.4.b show the corresponding spectrum, respectively. The higher height provides the larger compression force on crystal metarial; therefore, the percentage of emitted light is observed higher from 100 cm than other heights. With related to the principle of measurement TL intensity by drop tower system, there is an approximately 2.0 nm shift between photoluminescence and triboluminescence emission. This negligible value could be originated that there is a plexiglass gap between sample holder and fiber optic cable, which is light collector. When the ball falls, and hits the material; the emitted light is collected by fiber optic cable after light travelling into plexiglass material. The refractive index values for air at standard temperature and pressure (STP) and plexiglass are determined as 1.00 and 1.48, respectively. While the light travelling from higher refractive index medium to lower one, its fluctuation gains a speed with increasing frequency. Thus, the left shift on wavelength scale is observed. Additionally, the highest TL intensity of EuD_4TEA and $Cu(NCS)(py)_2(PPh_3)$ at 612.0 nm and 494.0 nm was contributed with respect to applied force in Figure 4.3.c and 4.4.c, respectively. The higher height cause loading larger forces onto TL material; therefore, the larger stress can lead to higher light radiation.

4.2. Characterization of Molecular Structures of TL Crystals

4.2.1. EuD_4TEA - $[Eu(C_{60}H_{48}O_2)_4]$ $[C_6H_{16}N]$

A specimen of $C_{66}H_{64}EuNO_8$, approximate dimensions 0.041 mm x 0.063 mm x 0.203 mm, was used for the X-ray crystallographic analysis. The X-ray intensity data were measured. The integration of the data using a monoclinic unit cell yielded a total of 10676 reflections to a maximum θ angle of 25.50° (0.83 Å resolution), of which 10676 were independent (average redundancy 1.000, completeness = 93.6%, R_{int} = 0.00%, R_{sig}

= 5.62%) and 10280 (96.29%) were greater than $2\sigma(F^2)$. The final cell constants of a = 9.0297(7) Å, b = 24.830(3) Å, c = 25.203(2) Å, β = 91.323(3)°, volume = 5649.2(9) $Å^3$, are based upon the refinement of the XYZ-centroids of reflections above 20 σ(I). The calculated minimum and maximum transmission coefficients (based on crystal size) are 0.8995 and 1.0000 (Table 1).

Chemical formula	$C_{66}H_{64}EuNO_8$		**Theta range for data collection**	2.26 to 25.50°	
Formula weight	1151.14 g/mol		**Reflections collected**	10676	
Temperature	100(2) K		**Independent reflections**	10676 [R(int) = 0.0000]	
Wavelength	0.71073 Å		**Max. and min. transmission**	1.0000 and 0.8995	
Crystal size	0.041 x 0.063 x 0.203 mm		**Structure solution technique**	direct methods	
Crystal system	Monoclinic		**Structure solution program**	SHELXT-2014 (Sheldrick 2014)	
Space group	P 1 21 1		**Refinement method**	Full-matrix least-squares on F^2	
Unit cell dimensions	a = 9.0297(7) Å	α = 90°	**Refinement program**	SHELXL-2014 (Sheldrick 2014)	
	b = 24.830(3) Å	β = 91.323(3)°	**Function minimized**	$\Sigma\, w(F_o^2 - F_c^2)^2$	
	c = 25.203(2) Å	γ = 90°	**Data / restraints / parameters**	10676 / 901 / 1376	
Volume	5649.2(9) $Å^3$		**Goodness-of-fit on F^2**	1.153	
Z	4		**Final R indices**	10280 data; I>2σ(I)	R1 = 0.0640, wR2 = 0.1801
Density (calculated)	1.353 g/cm^3			all data	R1 = 0.0679, wR2 = 0.1824
Absorption coefficient	1.167 mm^{-1}		**Weighting scheme**	$w=1/[\sigma^2(F_o^2)+139.3550P]$	
F(000)	2376			where $P=(F_o^2+2F_c^2)/3$	
			Absolute structure parameter	0.1(0)	
			Largest diff. peak and hole	0.800 and -1.642 $eÅ^{-3}$	
			R.M.S. deviation from mean	0.136 $eÅ^{-3}$	

Table 1: Structural Information about EuD_4TEA crystal

The structure was solved and refined using the Bruker SHELXTL Software Package, using the space group P 1 21 1, with Z = 4 for the formula unit, $C_{66}H_{64}EuNO_8$ (Figure 4.5).

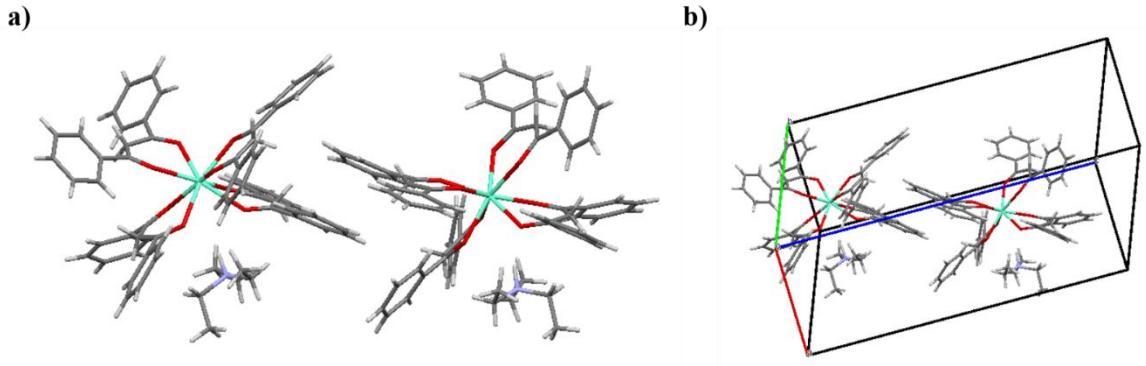

Figure 4.5. Molecular structure of Eu(III)-based crystal (a) and symmetry operation (b)

The final anisotropic full-matrix least-squares refinement on F^2 with 1376 variables converged at R1 = 6.40%, for the observed data and wR2 = 18.24% for all data. The goodness-of-fit was 1.153. The largest peak in the final difference electron density synthesis was 0.800 $e^-/Å^3$ and the largest hole was -1.642 $e^-/Å^3$ with an RMS deviation of 0.136 $e^-/Å^3$. On the basis of the final model, the calculated density was 1.353 g/cm^3 and F(000), 2376 e^-. The structure was refined as a 2-component twin, with twin contributions distinguished for processing using the program cell_now. TWINABS was used for scaling the data from the components. Bond lengths were calculated by using Mercury 3.7 programme in order to understand the accuracy of crystal structure (Table 2). Each bond length calculation is the clue and logic value for the conformation of twin formation.

Eu1-O1	2.365(16)	**Eu1-O8**	2.366(16)	**O16-C76**	1.29(3)	**C95-C96**	1.39(3)	**C108-C115**	1.53(3)	**C100-C105**	1.34(4)
Eu1-O3	2.369(15)	**Eu1-O6**	2.386(16)	**C95-C94**	1.40(3)	**C64-C65**	1.37(4)	**C100-C101**	1.41(4)	**C13-C14**	1.43(4)
Eu1-O2	2.385(17)	**Eu1-O7**	2.401(16)	**C64-C69**	1.40(4)	**C64-C61**	1.49(3)	**C112-C113**	1.34(4)	**O3-C33**	1.31(3)
Eu1-O4	2.402(13)	**Eu1-O5**	2.421(17)	**C62-C63**	1.41(3)	**C62-C61**	1.43(3)	**O7-C48**	1.25(3)	**C32-C33**	1.37(3)
O1-C1	1.30(3)	**O2-C16**	1.25(3)	**C91-C92**	1.38(4)	**C91-C94**	1.51(3)	**C33-C40**	1.50(4)	**C56-C57**	1.33(4)
O4-C18	1.27(3)	**O5-C3**	1.27(3)	**C63-C70**	1.52(3)	**C65-C66**	1.41(4)	**C56-C55**	1.44(4)	**C55-C60**	1.38(4)
C2-C1	1.36(3)	**C2-C3**	1.40(3)	**C78-C77**	1.42(4)	**C78-C85**	1.49(4)	**C55-C48**	1.50(3)	**C114-C113**	1.40(4)
C19-C20	1.39(4)	**C19-C24**	1.42(3)	**C67-C68**	1.35(4)	**C67-C66**	1.40(4)	**C82-C83**	1.37(4)	**C87-C88**	1.38(4)
C19-C18	1.50(3)	**C18-C17**	1.38(3)	**C73-C72**	1.39(4)	**C73-C74**	1.44(3)	**C116-C115**	1.36(3)	**C116-C117**	1.40(3)
C1-C10	1.50(3)	**C31-O6**	1.23(3)	**C80-C79**	1.37(3)	**C80-C81**	1.40(3)	**C38-C37**	1.38(4)	**C38-C39**	1.43(4)
C31-C32	1.39(3)	**C31-C34**	1.53(3)	**C75-C70**	1.35(4)	**C75-C74**	1.40(4)	**C27-C26**	1.36(4)	**C27-C28**	1.41(3)
C4-C5	1.39(4)	**C4-C9**	1.42(3)	**C76-C77**	1.38(3)	**C76-C79**	1.50(3)	**C57-C58**	1.47(4)	**C88-C89**	1.38(4)
C4-C3	1.47(3)	**C17-C16**	1.44(3)	**C72-C71**	1.37(3)	**C70-C71**	1.41(3)	**C37-C36**	1.41(4)	**C115-C120**	1.38(4)
C25-C30	1.37(4)	**C25-C26**	1.42(4)	**C79-C84**	1.42(3)	**C81-C82**	1.39(3)	**C90-C89**	1.40(4)	**C101-C102**	1.36(5)
C25-C16	1.49(4)	**C10-C15**	1.38(4)	**C96-C97**	1.39(3)	**C93-C92**	1.40(3)	**C117-C118**	1.34(3)	**C42-C41**	1.37(4)
C10-C11	1.42(3)	**C7-C8**	1.37(4)	**C93-C100**	1.49(3)	**C84-C83**	1.43(4)	**C42-C43**	1.41(4)	**C41-C40**	1.40(3)
C7-C6	1.40(3)	**C20-C21**	1.34(4)	**C97-C98**	1.40(3)	**C94-C99**	1.42(3)	**C118-C119**	1.44(4)	**C119-C120**	1.37(4)
C34-C39	1.35(3)	**C34-C35**	1.38(3)	**C85-C90**	1.38(4)	**C85-C86**	1.40(3)	**C29-C30**	1.38(4)	**C29-C28**	1.39(4)
C24-C23	1.39(3)	**C21-C22**	1.40(4)	**C106-C107**	1.34(4)	**C106-C109**	1.52(3)	**C40-C45**	1.41(3)	**C60-C59**	1.40(4)
C8-C9	1.35(4)	**C5-C6**	1.36(4)	**C107-C108**	1.45(3)	**O8-C46**	1.28(3)	**C45-C44**	1.38(4)	**C58-C59**	1.39(4)
C11-C12	1.40(4)	**C35-C36**	1.38(4)	**C46-C47**	1.36(4)	**C46-C49**	1.53(3)	**C43-C44**	1.43(4)	**C104-C105**	1.37(4)
C22-C23	1.35(4)	**Eu2-O9**	2.342(17)	**C109-C110**	1.38(3)	**C109-C114**	1.40(3)	**C104-C103**	1.41(4)	**C103-C102**	1.39(5)
Eu2-O10	2.370(18)	**Eu2-O12**	2.375(18)	**C47-C48**	1.43(3)	**C110-C111**	1.40(3)	**N2-C127**	1.49(3)	**N2-C128**	1.49(3)
Eu2-O11	2.384(17)	**Eu2-O15**	2.386(16)	**C50-C51**	1.38(3)	**C50-C49**	1.40(3)	**N2-C129**	1.50(3)	**C127-C130**	1.55(3)
Eu2-O13	2.390(17)	**Eu2-O14**	2.403(15)	**C69-C68**	1.38(4)	**C49-C54**	1.39(3)	**C128-C131**	1.48(4)	**N1-C121**	1.49(3)
Eu2-O16	2.407(16)	**O9-C61**	1.31(3)	**C12-C13**	1.39(4)	**C51-C52**	1.37(3)	**N1-C122**	1.51(3)	**N1-C123**	1.52(3)
O10-C78	1.28(3)	**O11-C91**	1.34(3)	**C52-C53**	1.36(3)	**C53-C54**	1.38(3)	**C121-C124**	1.50(4)	**C129-C132**	1.53(3)
O12-C93	1.27(3)	**O13-C106**	1.27(3)	**C15-C14**	1.37(4)	**C86-C87**	1.41(4)	**C122-C125**	1.53(4)	**C123-C126**	1.49(3)
O14-C63	1.26(3)	**O15-C108**	1.27(3)	**C111-C112**	1.39(4)	**C99-C98**	1.35(4)				

Table 2: Bond Length of each bond for the constructed EuD_4TEA crystal

4.2.2. $Cu(NCS)(py)_2(PPh_3)$ - $C_{29}H_{25}CuN_3PS$

A specimen of $C_{29}H_{25}CuN_3PS$, approximate dimensions 0.081 mm x 0.168 mm x 0.256 mm, was used for the X-ray crystallographic analysis. The X-ray intensity data were measured. The integration of the data using a monoclinic unit cell yielded a total of 29970 reflections to a maximum θ angle of 26.50° (0.80 Å resolution), of which 5319 were independent (average redundancy 5.635, completeness = 99.9%, R_{int} = 2.98%, R_{sig} = 2.89%) and 5206 (97.88%) were greater than $2\sigma(F^2)$. The final cell constants of a = 9.4006(4) Å, b = 15.1492(7) Å, c = 10.2153(4) Å, β = 116.9660(10)°, volume =

1296.61(10) $Å^3$, are based upon the refinement of the XYZ-centroids of reflections above 20 σ(I). The calculated minimum and maximum transmission coefficients (based on crystal size) are 0.9590 and 1.0000 (Table 3).

Chemical formula	$C_{29}H_{25}CuN_3PS$		**Theta range for data collection**	2.43 to 26.50°	
Formula weight	542.09 g/mol		**Index ranges**	-11<=h<=11, -19<=k<=19, -12<=l<=12	
Temperature	100(2) K		**Reflections collected**	29970	
Wavelength	0.71073 Å		**Independent reflections**	5319 [R(int) = 0.0298]	
Crystal size	0.081 x 0.168 x 0.256 mm		**Max. and min. transmission**	1.0000 and 0.9590	
Crystal system	monoclinic		**Structure solution technique**	direct methods	
Space group	P 1 21 1		**Structure solution program**	SHELXT-2014 (Sheldrick 2014)	
Unit cell dimensions	a = 9.4006(4) Å	α = 90°	**Refinement method**	Full-matrix least-squares on F^2	
	b = 15.1492(7) Å	β = 116.9660(10)°	**Refinement program**	SHELXL-2014 (Sheldrick 2014)	
	c = 10.2153(4) Å	γ = 90°	**Function minimized**	$\Sigma w(F_o^2 - F_c^2)^2$	
Volume	1296.61(10) $Å^3$		**Data / restraints / parameters**	5319 / 1 / 317	
Z	2		**Goodness-of-fit on F^2**	1.177	
Density (calculated)	1.388 g/cm^3		**Δ/σ_{max}**	0.001	
Absorption coefficient	1.007 mm^{-1}		**Final R indices**	5206 data; I>2σ(I)	R1 = 0.0185, wR2 = 0.0509
F(000)	560			all data	R1 = 0.0203, wR2 = 0.0665
			Weighting scheme	$w=1/[\sigma^2(F_o^2)+(0.0387P)^2+0.1000P]$	
				where $P=(F_o^2+2F_c^2)/3$	
			Absolute structure parameter	0.0(0)	
			Largest diff. peak and hole	0.308 and -0.360 $eÅ^{-3}$	
			R.M.S. deviation from mean	0.113 $eÅ^{-3}$	

Table 3: Structural Information about $Cu(NCS)(py)_2(PPh_3)$ crystal

The structure was solved and refined using the Bruker SHELXTL Software Package, using the space group P 1 21 1, with Z = 2 for the formula unit, $C_{29}H_{25}CuN_3PS$ (Figure 4.6).

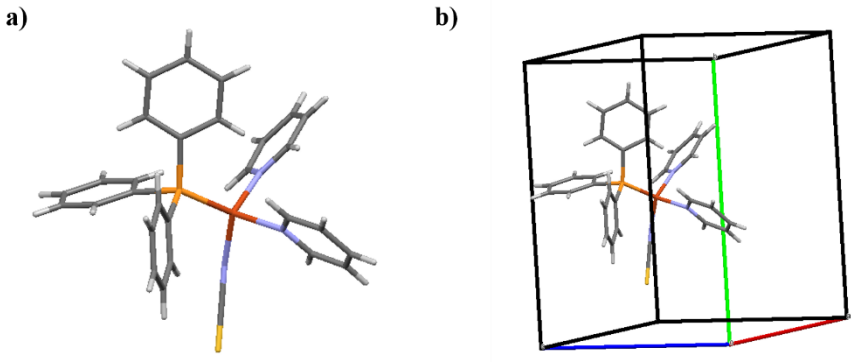

Figure 4.6. Molecular structure of Cu(I)-based crystal (a) and symmetry operation (b)

The final anisotropic full-matrix least-squares refinement on F^2 with 317 variables converged at R1 = 1.85%, for the observed data and wR2 = 6.65% for all data. The goodness-of-fit was 1.177. The largest peak in the final difference electron density synthesis was 0.308 $e^-/Å^3$ and the largest hole was -0.360 $e^-/Å^3$ with an RMS deviation of 0.113 $e^-/Å^3$. On the basis of the final model, the calculated density was 1.388 g/cm^3 and F(000), 560 e^-. Bond lengths were calculated by using Mercury 3.7 programme in order to understand the accuracy of crystal structure (Table 4). Each bond length calculation is the clue and logic value for the conformation of crystal formation.

Cu1-N3	2.010(3)	**Cu1-N2**	2.066(3)	**C19-H19**	0.95	**C23-C22**	1.386(4)	**C2-C3**	1.395(5)	**C2-H2**	0.95
Cu1-N1	2.092(2)	**Cu1-P1**	2.1945(8)	**C23-C18**	1.399(4)	**C23-H23**	0.95	**C24-C29**	1.395(4)	**C1-H1**	0.95
S1-C11	1.642(3)	**P1-C18**	1.826(3)	**C20-H20**	0.95	**C22-H22**	0.95	**C6-C7**	1.382(5)	**C6-H6**	0.95
P1-C12	1.827(3)	**P1-C24**	1.828(3)	**C26-C25**	1.388(4)	**C26-C27**	1.395(5)	**C3-C4**	1.370(5)	**C3-H3**	0.95
N1-C1	1.343(4)	**N1-C5**	1.350(4)	**C26-H26**	0.95	**C25-C24**	1.402(4)	**C29-C28**	1.396(4)	**C29-H29**	0.95
N2-C10	1.346(4)	**N2-C6**	1.347(4)	**C25-H25**	0.95	**C9-C8**	1.383(5)	**C27-C28**	1.382(5)	**C27-H27**	0.95
N3-C11	1.165(4)	**C10-C9**	1.385(4)	**C9-H9**	0.95	**C17-C16**	1.388(4)	**C5-C4**	1.387(5)	**C5-H5**	0.95
C10-H10	0.95	**C12-C13**	1.396(4)	**C17-H17**	0.95	**C14-C15**	1.392(5)	**C8-C7**	1.390(5)	**C8-H8**	0.95
C12-C17	1.402(4)	**C21-C22**	1.388(4)	**C14-C13**	1.395(4)	**C14-H14**	0.95	**C15-H15**	0.95	**C28-H28**	0.95
C21-C20	1.391(5)	**C21-H21**	0.95	**C13-H13**	0.95	**C16-C15**	1.383(5)	**C7-H7**	0.95	**C4-H4**	0.95
C19-C20	1.384(4)	**C19-C18**	1.400(4)	**C16-H16**	0.95	**C2-C1**	1.378(5)				

Table 4: Bond Length of each bond for the constructed $Cu(NCS)(py)_2(PPh_3)$ crystal

4.3. Quantitative Triboluminescence of Composite Films

TL performance of composites were investigated by using drop tower system which was defined in Figure 3.7. The spectral features were given in Figure 4.7. with respect to two main parameters: i) type of process and ii) chemistry of polymer.

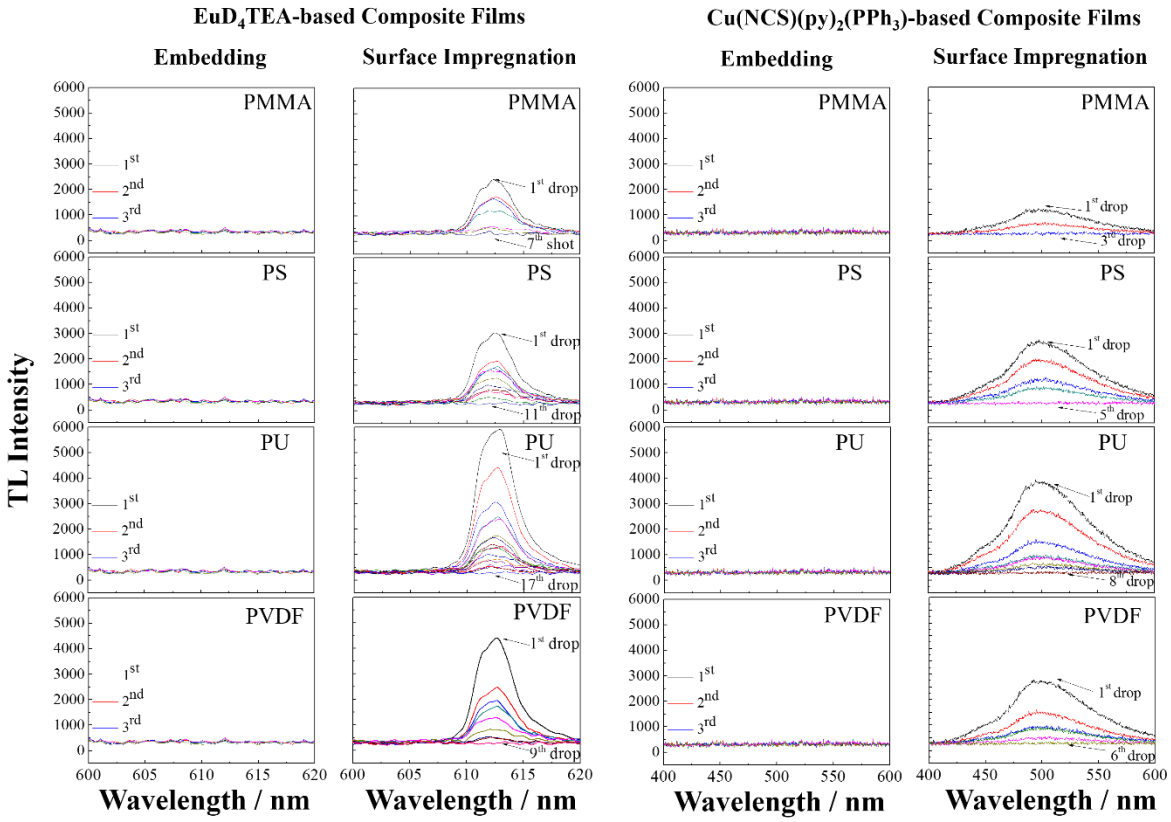

Figure 4.7. TL emission spectra of TL/transparent polymer composite films with respect to both type of process and chemistry of polymers which were indicated on graph into panel

In experimental difference, the prior embedding composites have no TL response under mechanical force. The further surface impregnated composites show various TL performance in terms of number of drop. This incoherence may be originated from the physical form of crystal in composites for both TL materials. The crystalline particles were molecular dissolved in polymer solution in embedding process (liquid form); however, the crystal dipsersion in water was used for surface impregnation process (solid form). The dissolution of crystalline particles in polymer solution by the effect of aprotic polar solvent DMF can cause degradation of crystals under mechanical force by triggering the metal-nitrogen bonds of $–N(CH_2CH_3)_3$ for EuD_4TEA and –NCS for

$Cu(NCS)(py)_2(PPh_3)$. Therefore, their TL properties were expired. Surface impregnated composites having different repetition as a function of the number of drops were associated with the chemistry of polymer. The repetition for Eu(III)-based composites is 7, 11, 17, and 9 for PMMA, PS, PU, and PVDF respectively. The same order is 3, 5, 8, and 6 for Cu(I)-based composites.

The increase in repetition cycle with respect to corresponding polymer for both crystals is identical and PU-based composites have higher stability towards the application of mechanical force. Moreover, Figure 4.8. also defines the lost on emitted TL for the surface impregnated composites.

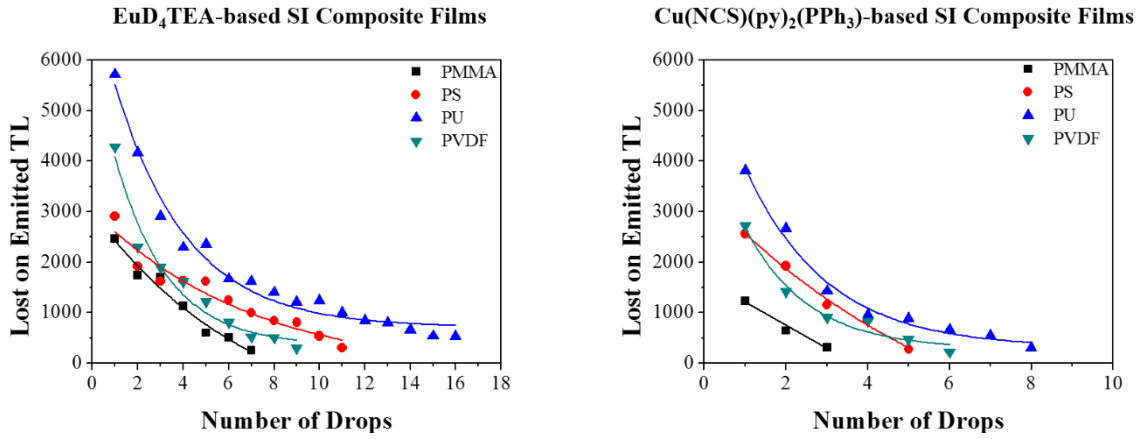

Figure 4.8. The lost on emitted TL with respect to number of drop for both crystal-based composites, EuD_4TEA (a) and $Cu(NCS)(py)_2(PPh_3)$ (b)

The emitted intensity after the first drop applied exhibits different value and depends on both crystal and polymer. The first intensities for Eu(III)-based composites are 6000, 3500, 3000, and 4500 au. in the order of PMMA, PS, PU, and PVDF respectively shown in the left side of Fig. 4.8. This order is respectively 4000, 2750, 1500, 3000 au. for Cu(I)-based composites shown in the right side of Fig. 4.8.

The increase in the number of drops cause the decrease in emitted TL. In the comparison of the first TL intensities of crystals for PU-based composites, the size of particles should be indicated to understand the effect of particle size on TL performance. Therefore, SEM images were taken for no stress, and after applied forces as a function of the increase in number of drops. Additionally, the images were converted to size distribution graph as readily data by ImageJ and the panel for both crystals size was shown in Figure 4.9.

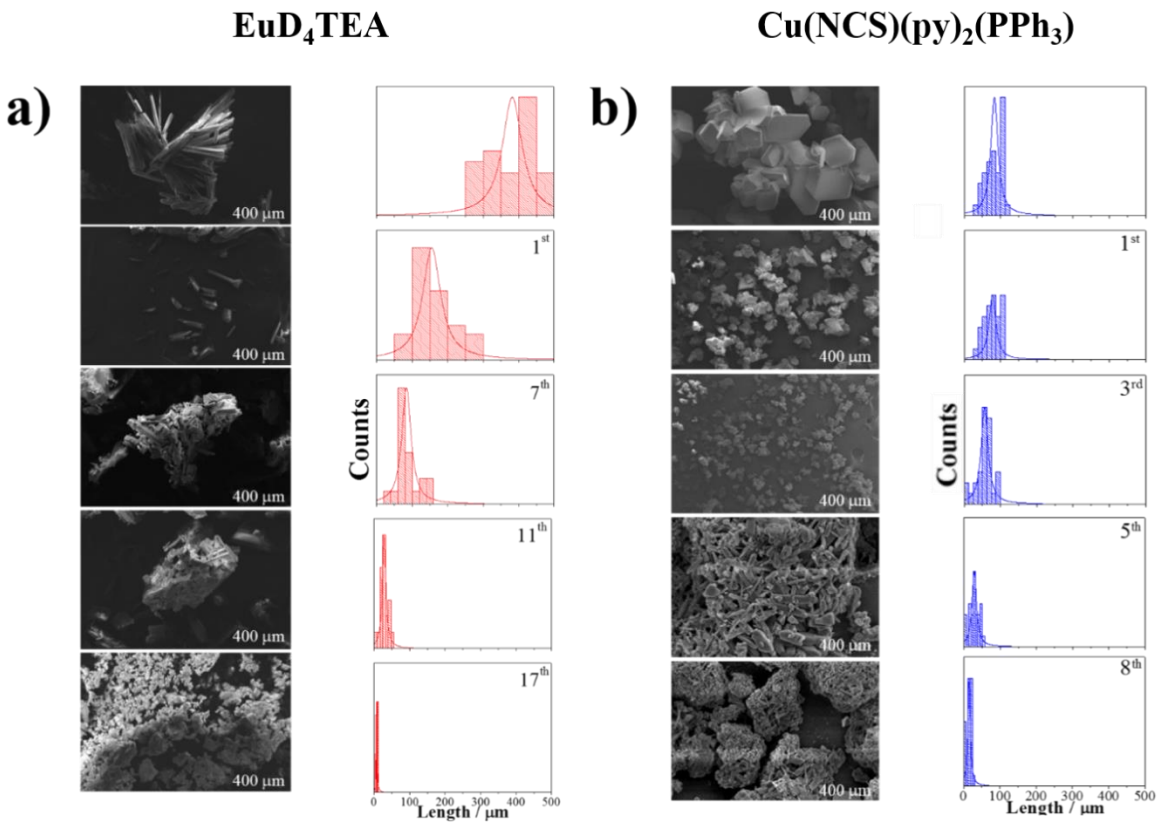

Figure 4.9. The change in crystal size distribution of surface impregnated composite by the increase in the number of ball shot with respect to SEM images of both crystals: EuD_4TEA (a), and $Cu(NCS)(py)_2(PPh_3)$ (b)

The average size distribution varies as 150, 120, 100, 80, and 30 μm for no-stress and from 1st, 7th, 11th, and 17th ball shots for Eu(III)-based composite (Figure 4.9.a). The average size distribution varies as 80, 60, 50, 30, and 20 μm for no-stress and 1st, 3rd, 5th, and 8th for Cu(I)-based composites (Figure 4.9.b). It is obviously seen that the average particle size of EuD_4TEA is is larger than the average particle size of $Cu(NCS)(py)_2(PPh_3)$. Moreover, when the number of drop increases, the size of particles become smaller for both cases.

As a result, the emitted TL intensity is getting lower. The reason is that when the mechanical force is applied, the particle size of crystalline particles is becoming smaller. This effect causes the decrease in the molecular interaction of particles. The less particle interaction leads to produce lower emitted TL. Another reason may be originated from the quantum efficiency of emitted particles. The correlation between radiative and non-radiative emission simply determines the quantum efficiency. When the size of particles become smaller, the surface area of particles increases. Moreover, the electron-surface

scattering increase by the decrease in the crystal size. The relaxation of electron-phonon coupling decreases and the time for the relaxation of photo-excited electron gains speed from milisecond to femtosecond.(Link and El-Sayed 2000) The increase in relaxation time causes to the significant increase in non-radiative decay than radiative decay; therefore, the decrease in emitted intensity occurs. This result is completely consistent with the notion that the change in the first visual inspection of the intensities light decay and the stability of composite are directly related to the size of crystalline particles.

4.3.1. Microscopic Characterization of Composite Films

Not only the size of particles but also physical properties of polymers and polymer-crystal relation, both are really important to define TL performance of composites. The surface topography of polymer matrices is desired to provide high effective surface-particle interaction at the expense of TL performance in loaded applied force. In terms of topographic aspect, the porosity of thin polymer film is significant physical property which impacts the quality and utility of solid-phase polymer. The reason is that AFM helps to investigate the surface topograhies of transparent polymer films and the images were shown in Figure 4.10. The average roughness values can be ordered as 0.272 nm, 2.18 nm, 12.4 nm and 18.8 nm for PMMA, PS, PU, PVDF. It is worth pointing out that the surface of thin film PVDF has rougher surface than the other thin-film polymers. On the other hand the depth of PU surface is higher than other polymers. Difference in roughness depth may be originated from the breath figure formation.(Deepa and Jayakannan 2007) This methodology is known as the more hydrophobic solid surface allows to the spontaneously coagulation of solvent droplets with non-zero contact angle on the polymer surface at annealing process. PU has thermodynamically higher incompatibly than PVDF, PS and PMMA due to the fact that PU consists of high proportion of ether-oxygen and urethane-based functional groups. The reason is that high percentage micro domain segregation was formed on the thin film PU.

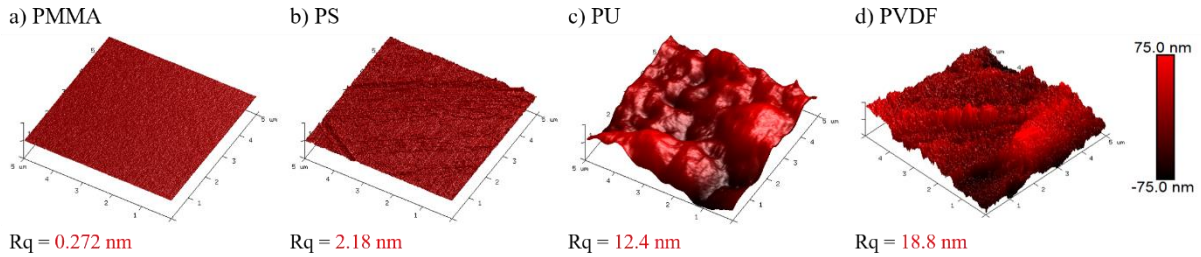

Figure 4.10. AFM images of thin-film polymer surface:
PMMA (a), PS (b), PU (c), and PVDF (d)

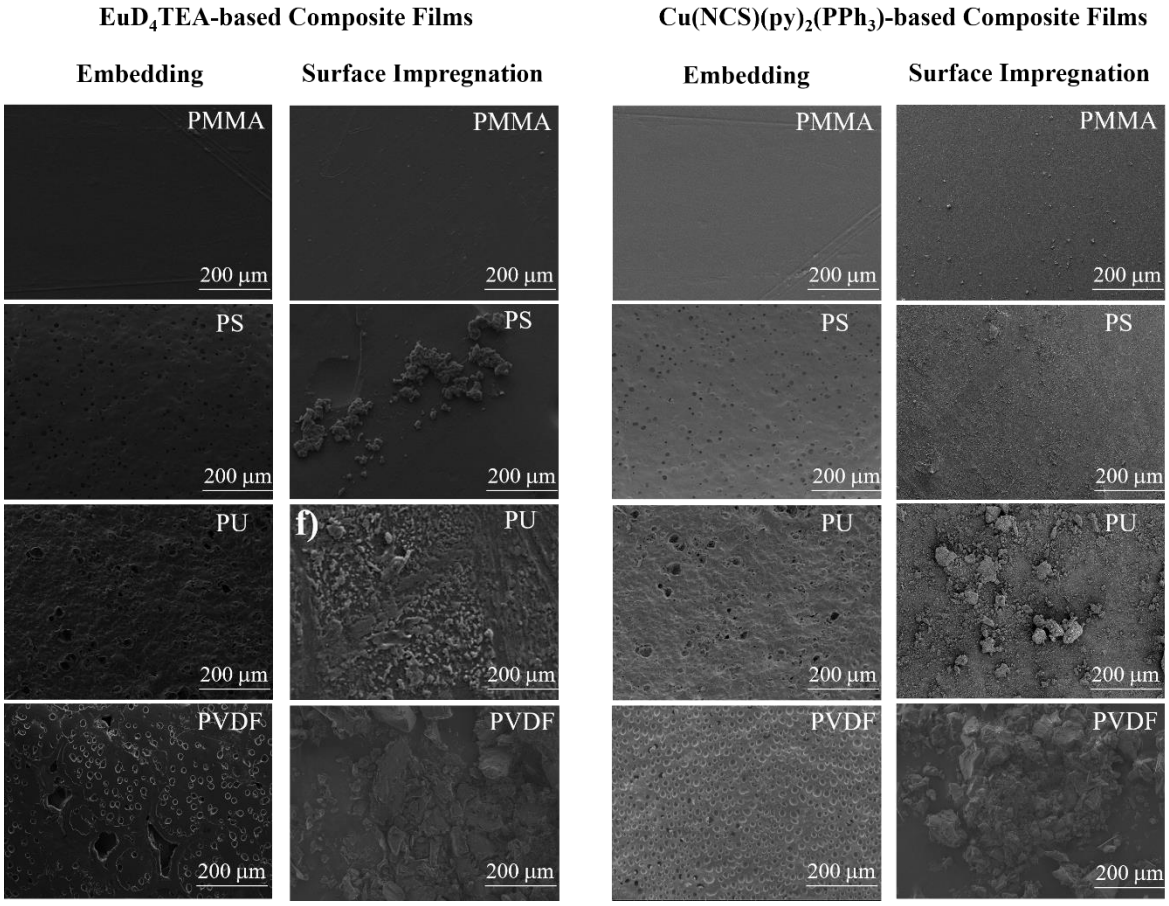

Figure 4.11. SEM images of TL / transparent polymer composite films with respect to both type of process and chemistry of polymers which were indicated on graph into panel

The incongruity in the roughness of thin film polymer, which otherwise may have some physical dimensions, can considerably influences the TL performance of composites in terms of stability towards the application of mechanical force. On the other hand, the stability of TL performance is directly related to the percentage of loaded crystalline particles. The much porous surface leads to the increase amount of the loaded

particles onto thin film polymer. SEM images of composites, which were indicated in Figure 4.11., were taken to support not only the roughness of transparent thin films but also emphasizing the percentage of loaded crystalline particles on the surface of polymer film.

In embedding process, the determined mass of particles were completely dissolved in polymer solution. However, the thin films were treated by crystal dispersion in water at the surface impregnation process.

The reason is that the percentage of loaded crystalline particles by weight for each surface impregnated composite was calculated by using the amount of extracted dispersion than the whole amount of treated solution. The percentage of impregnated particles on thin film was given in Figure 4.12. by repeating this process three times for each composite.

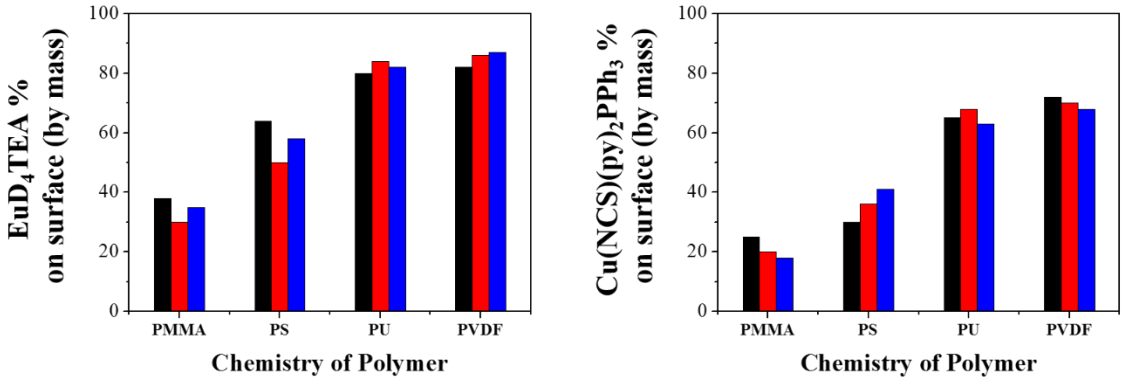

Figure 4.12. Loaded crystal percentage by weight on the surface of polymer films for the surface impregnated composites with respect to chemistry of polymers for EuD_4TEA (a) and $Cu(NCS)(py)_2(PPh_3)$ (b)

The average amount of loading TL particles of impregnated crystalline particles on the Eu(III)-based composite films are 87%, 85%, 55%, and 30% for PVDF, PU, PS, and PMMA, respectively. There is a similar trend for the same order as 70%, 65%, 32%, and 20% for Cu(I)-based composites. In the case of 85 wt.% loaded for Eu(III)-based composite and 65 wt.% loaded for Cu(I)-based composite, the intensity of first emitted TL of PU-based surface impregnated composites has the highest for both case even though the impregnated crystalline particles are less than PVDF film surface. This result may be originated from the optical incoherence between PU and PVDF thin-film surface. PVDF is much opaque surface than completely transparent PU surface which is shown in

Figure 4.13. Additionally, PU has chemical affinity to load higher amount of crystalline particles due to containing aromatic group.

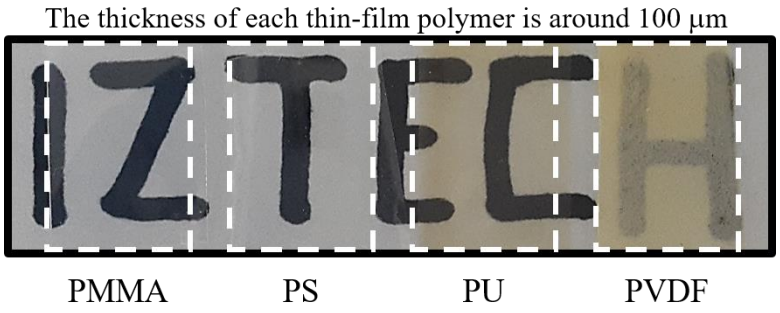

Figure 4.13 Transparency test for thin-film polymer

	EuD_4TEA-based Composite Films		$Cu(NCS)(py)_2(PPh_3)$-based Composite Films	
	TL/TL+polymer % by mass		TL/TL+polymer % by mass	
Type of Polymer	Embedded	Surface Impregnated	Embedded	Surface Impregnated
PMMA	14	5	14	3
PS	14	8	14	5
PU	14	12	14	10
PVDF	14	13	14	11

Table 4.5. TL/TL+polymer percentage by mass for TL/polymer based composite films

Additionally, the amount of TL/TL+polymer percentage by mass was calculated by using mass percentage amount of loaded crystalline particles and the mass amount of impregnation solution in the experiment part. Table 4.5. exhibit the ratio for each type composite. It is assumed that molecular dispersion of crystalline particles in embedding process, all crystalline were embedded in the polymer film. On the other hand, the loaded crystalline particles were used to calculate the ratio for surface impregnated composites. It is obviously seen that the mass ratio increases from PMMA to PVDF for both cases.

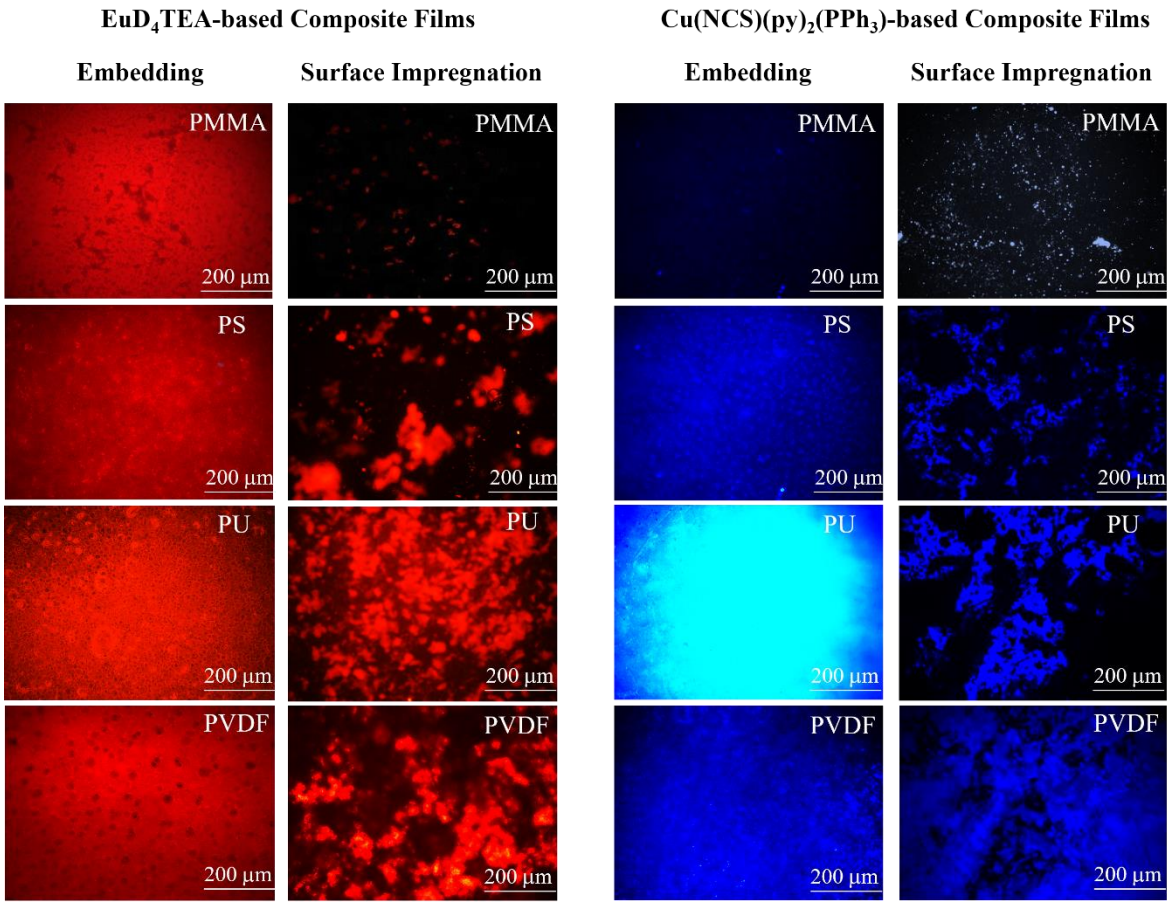

Figure 4.14. FM images of TL / transparent polymer composite films with respect to both type of process and chemistry of polymers which were indicated on graph into panel

Moreover, all results reveal that there is a significant effect of both type of process and chemistry of polymer on the TL performance of composites. In detail, the physical property of polymer cause to the high percentage of deposited crystalline particles; therefore, the high-weight-percentage-loaded composite exhibits the highest TL intensity with great stability and longer decay time in the presence of repeated mechanical action.

The TL crystals integrated thin film polymers were further examined by FM upon the excitation with UV-light (λ=365 nm). Figure 4.14. exhibits the bright field fluorescence microscopy images of composite films.

It is known that the polymer which were used have no PL emission. In terms of surface impregnation process, the signals of red emission from Eu(III)-based composites and blue emission from Cu(I)-based composites were observed indicating that the crystalline particles were fairly and uniformly distributed in the hosting of PU and PVDF

polymer matrix for both cases in Figure 4.14. Separately, the emission signals for both embedded composites show color differences. While the signals of Eu(III)-based composites vary from orange to red in the change of PMMA, PS, and PU, and it turns back the same colour of PS-based composite film for PVDF-based composites. The emission signals of Cu(I)-based composites change from dark to light blue from PMMA to PU, and it turns back the same colour of PS-based composite film for PVDF-based composites.

This photo-luminescent change induced by the dissolution of TL crystals in polymer solution may account for the changes in the characteristic of polymer compared to the surface impregnated composites. The back-bone chains in polymers consists of acrylic, styrene, urethane, fluorine groups for PMMA, PS, PU, and PVDF respectively. It seems that the conjugation of polymers increases by the effect of delocalized π-electrons resulting PL color change in the emitted component. The excess of electron-donor groups in polymer interchanged with electron-poor acceptor group in the non-polar solvent can directly effected on the number of valence electrons. When π-electrons donates to PL material, the band gap between valence and conduction states decreases. Thus, the luminescent signal forms in the lower energy. Red shift for Eu(III)-based composite and blue shift for Cu(I)-based composite occur by the effect of decreasing energy with the increasing wavelength scale.

In terms of TL performance of composite materials, the size of crystal particles, the porosity of thin film polymer surface, impregnated percentage of crystalline particles, and PL characteristics of composites were investigated. When these all aspects were taken into consideration, even though the fixed [TL] (14 wt.% in polymer) is good enough to take TL response from the surface impregnated composites, embedding composites show no TL emission after the application of mechanical force. The reason is that the change of [TL] in host material might be contributed to the TL performance except the dissolution of crystals into polymer solution.

4.3.2. [TL] effect on Embedded Composites

Figure 4.14. exhibits a panel of PU-based embedded composites as a function of [TL] from 10% to 99%. FM images of composites were taken to understand the effect of embedded particles into polymer matrix in Figure 4.15.a and 4.15.c for Eu(III) and Cu(I) based composites, respectively. In both cases, the more embedded particles lead to lower light emission under UV light; therefore, the same result was taken under the effect of loaded particles like the effect of polymer which was indicated in Figure 4.12. The TL emission yield for each composite film was measured by usind drop tower system under the application of one drop and the results were shown in Figure 4.15.b and 4.15.d for Eu(III) and Cu(I) based composites, respectively.

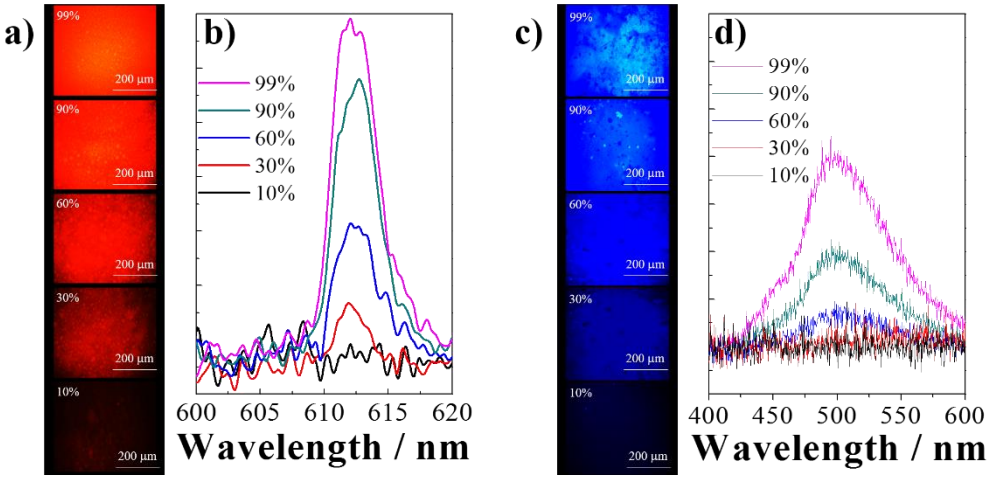

Figure 4.15. Characterization panel for the effect of [TL] in embedded composite films with respect to FM (a and c) and TL emission spectra (b and d) which were indicated on graph in panel

It is obivously seen that when [EuD_4TEA] is equal or more than 30% in PU solution, the composite started to give triboluminescence response toward the application of compression force by one ball shot. In terms of $Cu(NCS)(py)_2(PPh_3)$, when the [TL] is equal or more than 60% in PU solution, the composite give TL radiation. As a result, it was verified that there is a threshold for [TL] in polymer for embedding process.

4.4. Quantitative Triboluminescence of Composite Electrospun Fibers

Integration of TL crystals with electrospun fibers have been done due to the fabrication of three different PMMA, PS, PU, and PVDF electrospun fibers by using electrospinning instrument, which was illustrated in Figure 3.4. Two main strategies were employed for the preparation of TL/nanofibrous composites. The former was prepared the fluorescent fibers during electrospinning process, the latter was employed as the hybrid fibers after electrospinning process by impregnating of crystalline particles onto fiber surface. These two methodologies are the same approach as embedding and surface impregnation processes which were used to obtain composite films.

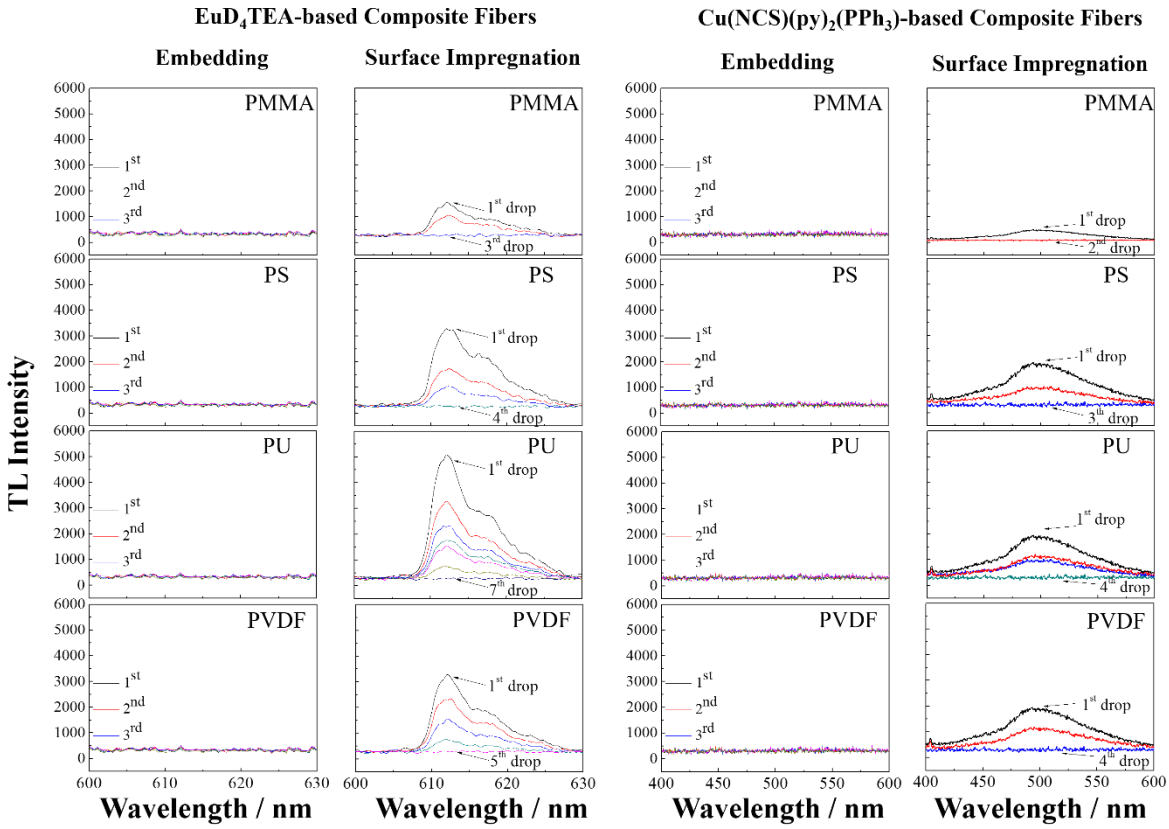

Figure 4.16. TL emission spectra of TL/electrospun fiber composites with respect to both type of process and chemistry of polymers which were indicated on graph into panel

TL performance of nanofibrous composite was investigated by using drop tower system and the spectral features were given in Figure 4.16. The similar performance as a function of number of drop was taken when fiber composites are compared with film composites. Embedding composites have no TL response because of the same reason

which was defined in composite films. On the other hand, surface impregnated composites having different repetition as a function of the number of drops were associated with the chemistry of polymer.

The repetition for Eu(III)-based composites is 3, 4, 7, and 5 for PMMA, PS, PU, and PVDF respectively in Figure 4.15. The same order is 2, 3, 4, and 3 for Cu(I)-based composites. The repetation cycle with respect to corresponding polymer for both crystals is identical but the stability of each composite is approximately half of the composite films. The main reason of lower emitted intensity and narrow dynamic range for stability may be originate from the optical incoherence between fiber and film. Even though the polymer film is transparent, the fiber mat is completely opaque and it causes a scatter media. Thus, the emitted TL is diminished and the intensity of collected light will be reduced.

The increase in repetition cycle with respect to corresponding polymer for both crystals is identical and PU-based composites have higher stability towards the application of mechanical force. Moreover, Figure 4.17. also defines the lost on emitted TL for the surface impregnated composites.

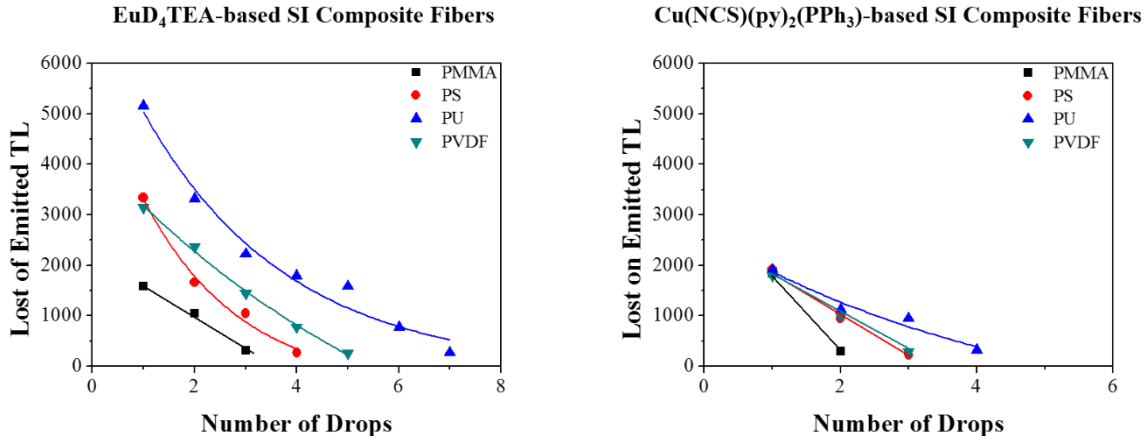

Figure 4.17. The lost on emitted TL with respect to number of drop for both crystal-based composites: EuD_4TEA (a) and $Cu(NCS)(py)_2(PPh_3)$ (b)

The emitted intensity after the first drop applied exhibits different value and depends on both crystal and polymer. The first intensities for Eu(III)-based composites are 5000, 3500, 1750, and 3000 au. in the order of PMMA, PS, PU, and PVDF respectively shown in the left side of Fig. 4.17. This order is respectively more or less the same as 2000 au. for Cu(I)-based composites shown in the right side of Fig. 4.17.

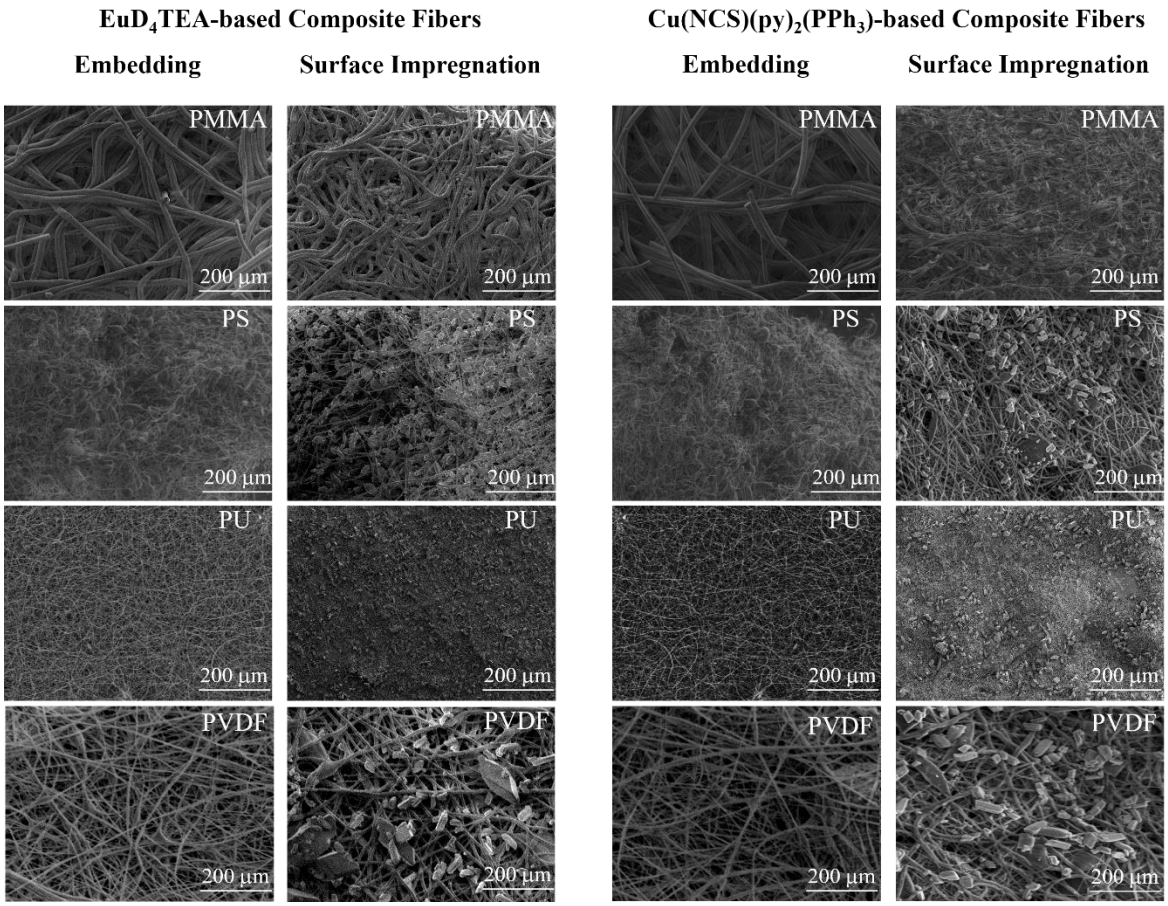

Figure 4.18. SEM images of TL/electrospun fiber composites with respect to both type of process and chemistry of polymers which were indicated on graph into panel

In the microscopic characterization of neat fiber network and TL integrated composite fibers, SEM images were investigated and shown in Figure 4.18. In fiber composites, the physical properties of electrospun fibers are the key for TL performance. It seems that PU fiber network is more uniform than PMMA, PS, and PVDF even though the polymer solutions were prepared in the same solvent and they exposed the same electro-spinning parameters. Additionally, the diameters of fibers were obtained as distributed graph and shown in Figure 4.18. The average fiber diameter is around 300 nm, 100 nm, 30 nm and 80 nm for PMMA, PS, PU, and PVDF electrospun network. The smallest wickerwork surface property of PU with a nano-meter scale connection provides to obtain have high surface-to-volume ratio for the integration of crystalline particles for surface impregnated composites.

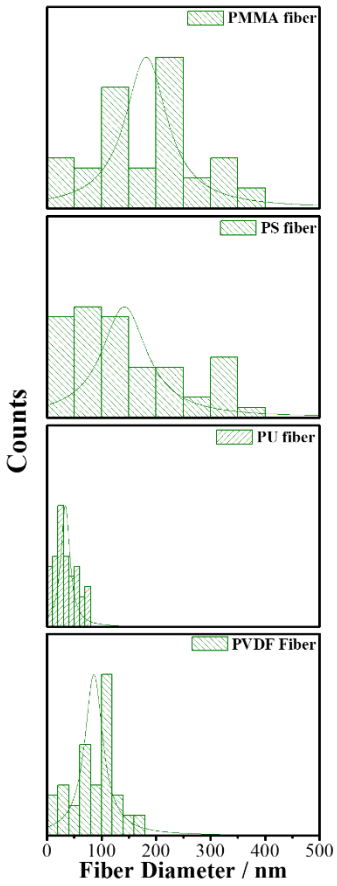

Figure 4.19. The Diameter of Electrospun Fiber: PMMA, PS, PU, and PVDF

Moreover, the loaded percentage of TL crystals on the surface of fiber mats were calculated by using the same methodology as the film composites and the results were shown in Figure 4.20.

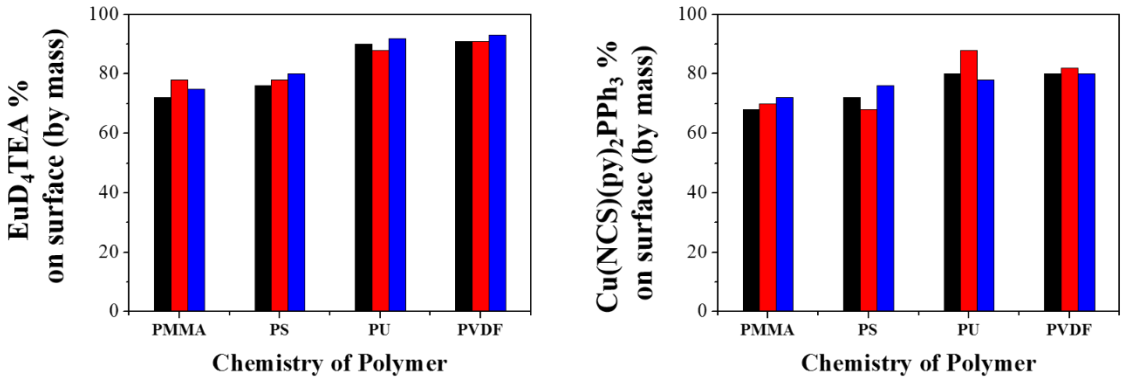

Figure 4.20. Loaded crystal percentage by weight on the surface of nanofiber for the surface impregnated composites with respect to chemistry of polymers for EuD_4TEA (a) and $Cu(NCS)(py)_2(PPh_3)$ (b)

The average of impregnated crystalline particles on the Eu(III)-based composite fibers are 90%, 88% 78%, 75% for PU, PVDF, PS, and PMMA, respectively. There is a coherence for the same order as 85%, 75%, 72%, and 70% for Cu(I)-based composites. In the case of 90 wt.% loaded for Eu(III)-based composite and 85 wt.% loaded for Cu(I)-based composite, the intensities of first emitted TL of PU-based surface impregnated composites are the highest for both case. When the percentage of loaded crystalline particles were compared for both film and fiber composite, the each fiber composite impregnated by the higher amount of TL crystals rather than film composite. However, the first TL intensity and the stability of fiber composite is nearly half of the film composite. The first reason which was discussed in morphologic characterization as the opaque property of fiber network. Another reason fiber mats have layer formation but thin film is one layer. Layer-by-layer stacking mats causes the sepreading of crystal particles not only on the surface but also inside the fiber mats. When the mechanical force is applied, number of total emitted crystal particles which were exposed to applied force is lower than the thin film composite. This layer formation can cause to the reduce in emitted TL.

Additionally, the amount of TL/TL+polymer percentage by mass was calculated by using mass percentage amount of loaded crystalline particles and the mass amount of impregnation solution in the experiment part. Table 4.6. exhibit the ratio for each type composite. It is assumed that molecular dispersion of crystalline particles in embedding process, all crystalline were embedded in the polymer film. It is obviously seen that the mass ratio increases from PMMA to PU and PVDF for both cases. The last two show the same amount.

	EuD_4TEA-based Composite Fibers		$Cu(NCS)(py)_2(PPh_3)$-based Composite Fibers	
	TL/TL+polymer % by mass		TL/TL+polymer % by mass	
Type of Polymer	Embedded	Surface Impregnated	Embedded	Surface Impregnated
PMMA	14	11	14	10
PS	14	12	14	10
PU	14	13	14	12
PVDF	14	13	14	12

Table 4.6. TL/TL+polymer percentage by mass for TL/polymer based composite fibers

The TL crystal integrated electrospun fiber composite were further examined under the FM upon the excitation with UV light (λ=365 nm). Figure 4.21. show the bright field fluorescence microscopy images of composites. Similarly, the color of emitted light is the same in the case of composite film for both TL-based fiber composites. For the surface impregnated composites, the distribution of TL crystals can be seen not only onto the surface of fibers but also in the layers of fiber network.

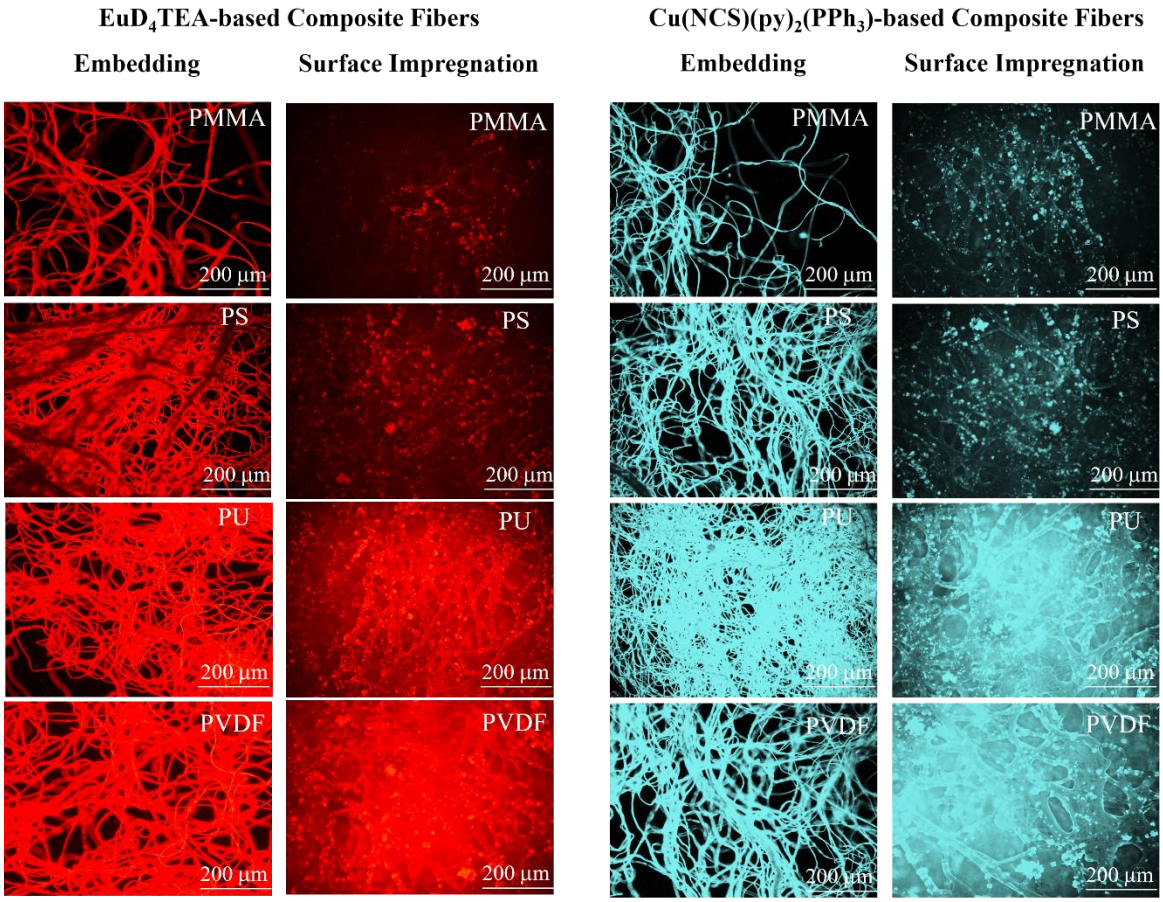

Figure 4.21. FM images of TL / nanofibrous polymer composite films with respect to both type of process and chemistry of polymers which were indicated on graph into panel

The small-sized connected network of PU electrospun fibers have the brighest emitted color of red for Eu(III)-based and blue for Cu(I)-based composites rather than PMMA, PS, and PVDF based composites. Additionally, the crystal particles can be easily detectable. Moreover, the fluorescence color of PU-based composites is highly bright and separating of emitted light surrounding of area due to the high-TL crystals loaded. In

terms of embedded composites, the same color incoherence were observed for both crystals. π-electrons resulting e-donor groups into system; therefore, the signals of luminescent colors were detected on the right-shift-wavelength.

4.5. Quantitative Triboluminescence of EuD_4TEA/PS Nanobead Composite

The synthesized PS NPs and EuD_4TEA/PS NPs composites were investigated by SEM to understand morphological change. PS NPs are spherical form and they were at nano-scale (Fig. 4.22a). The average size diameter of nanoparticles is around 35 nm (Fig. 4.22c). The TL/bead composite showed that the PS nanospheres were surrounded by crystalline structures (Fig. 4.22b). In other words, Eu(III)-based crystals were growth on the nanoparticles. The nanoparticles provided to the stabilized and constructed the crystals. The TL emission of equal amounts of PS NPs, bulk EuD_4TEA crystals, and EuD_4TEA/PS NPs by weight were obtained by drop tower system and the spectral features were shown in Figure 4.22.d. TL response of both PS NPs and EuD_4TEA/PS NPs were done by drop tower system.

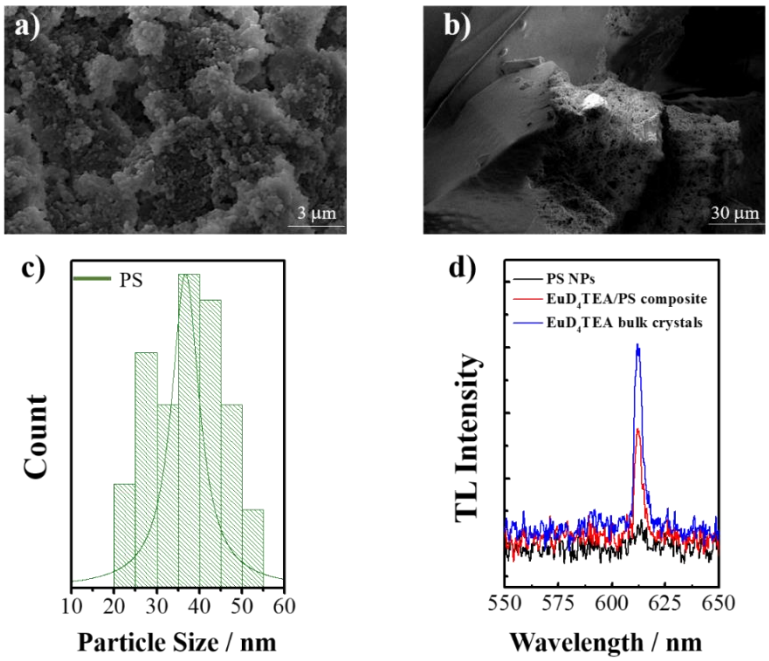

Figure 4.22. SEM images of both PS NPs (a) and EuD_4TEA/PS Beads (b), Particle Size Distribution of PS nanobeads (c), and TL response of PS NPs and EuD_4TEA/PS NPs composite (d)

In the comparison of emitted TL intensity, PS nanoparticles show no TL emission as expectedly; however, EuD_4TEA/PS nanobead composite show significant TL emission. The less emitted TL intensity by composite beads than bulk crystal may be originate from the formation of light in scattery medium.

4.6. Piezoelectricity of TL/polymer composite films

In the measurement of piezoelectric voltage, each slot was set to 250 nanoseconds (ns) in the range of 0 to 4000 unit. Each slot occupies 0.625 ns. The interval for piezoelectric voltage was determined as 300 ns in the range of 1100 to 1400 unit. From 0 to 1100, the measurement voltage was called as piezo trigger to stabilize the system control and be sure that trigger point is fixed at 0 point. The operating voltage was set peak to peak separation from +30 mV to -30 mV. It is well established that piezo materials produced electrical voltage after the application of mechanical forces. It behaves like a tiny battery with a positive charge on one face of crystal and negative charge on the opposite face; therefore, the current flows between these edges. The applied mechanical stress causes the deformation in shape of crystals and the voltage is produced across its opposite faces.

The highest voltage separation was recorded as the maximum produced piezoelectric voltage. When the mechanical stress is carried out, the trigger is pulled around 30 ns (Figure 4.23) for measurement interval and starts to accelerate. For each case, the highest peak-to-peak separation providing by distributed electrical charges appears between 150 ns to 165 ns. After the time of 165 ns, the effect of mechanical stress on piezoelectric materials was done, and the produced electrical charges started to be balanced; therefore, the oscillation has left and ended.

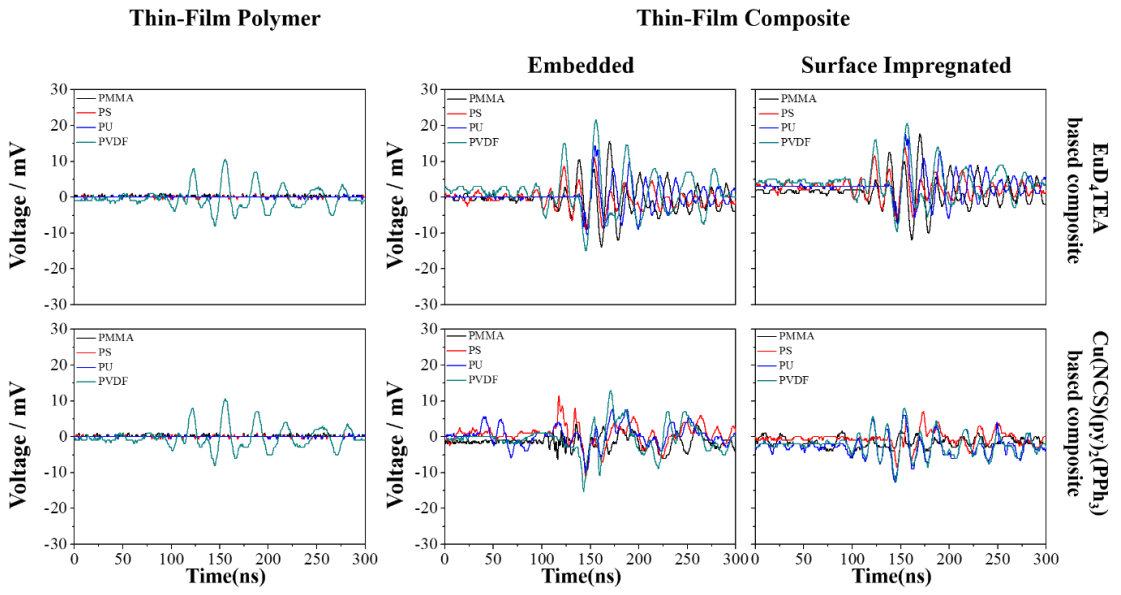

Figure 4.23. Piezoelectric Voltage Measurement for both thin-film polymer and TL/polymer composite films

a)

Type of Thin-film Polymer	Minimum Voltage	Maximum Voltage	Total Voltage (mV)
PMMA	0	0	0
PS	0	0	0
PU	0	0	0
PVDF	-7,54	10,49	18,03

b)

Type of Thin-Film Embedded Composite	Minimum Voltage	Maximum Voltage	Total Voltage (mV)
PMMA/EuD_4TEA	-8,7	8,3	17
PS/EuD4TEA	-8	10	18
PU/EuD4TEA	-10	14	24
PVDF/EuD4TEA	-14,68	21	35,68

c)

Type of Thin-Film SI Composite	Minimum Voltage	Maximum Voltage	Total Voltage (mV)
PMMA/EuD_4TEA	-5,44	9,7	15,14
PS/EuD4TEA	-5,81	12,74	18,55
PU/EuD4TEA	-6,99	16,71	23,70
PVDF/EuD4TEA	-9,39	20,43	29,82

d)

Type of Thin-Film Embedded Composite	Minimum Voltage	Maximum Voltage	Total Voltage (mV)
PMMA/$Cu(NCS)(py)_2(PPh_3)$	-4,58	2,42	7
PS/$Cu(NCS)(py)_2(PPh_3)$	-5,20	3,65	8,65
PU/$Cu(NCS)(py)_2(PPh_3)$	-5,35	7,39	12,74
PVDF/$Cu(NCS)(py)_2(PPh_3)$	-10,63	12,67	23,3

e)

Type of Thin-Film SI Composite	Minimum Voltage	Maximum Voltage	Total Voltage (mV)
PMMA/$Cu(NCS)(py)_2(PPh_3)$	-2,57	1,02	3,59
PS/$Cu(NCS)(py)_2(PPh_3)$	-8,15	3,34	11,49
PU/$Cu(NCS)(py)_2(PPh_3)$	-10,21	5,66	15,87
PVDF/$Cu(NCS)(py)_2(PPh_3)$	-12,89	7,62	20,51

Table 4.7. The values of minimum, maximum, and total voltage for each thin-film polymer and thin-film polymer composite

The piezoelectric measurement of both thin-film polymer and TL/polymer composite films were done by using the combined system of drop tower system and digital storage oscilloscope which was defined in Figure 3.9. In the piezoelectric voltage change on thin-film polymers, only PVDF films exhibit piezoelectricity after the application of mechanical force (Figure 4.23). The reason is that the applied voltage cause the disturbance on periodicity of the unit cell of PVDF solid membrane and it discharges as voltage response. PMMA, PS, and PU thin-film polymers shows no response. In the piezoelectric change on thin-film TL/polymer composites, the piezoelectric behaviour of triboluminescent crystalline particles lead to obtain voltage change for each composite. There is a trend for both TL crystals the percentage of produced voltage increases from PMMA to PVDF.

Table 4.7. shows the minimum, maximum, and total voltage change of thin-film polymer and thin-film composites. The total voltage change on thin film polymers is 0,

0, 0, and 18.03 mV for PMMA, PS, PU, and PVDF, respectively in Table 4.7a. The total voltage change on thin-film for Eu(III)-based embedde composites are 17, 18, 24, and 35,68 mV for PMMA, PS, PU, and PVDF, respectively (Table 4.7b). The order has identical results for Eu(III)-based surface impregnated composites as 15.14, 18.55, 23.70, and 29.82 mV (Table 4.7c).

The total voltage change on thin-film for Cu(I)-based embedde composites are 7, 8.65, 12.74, and 23.3 mV for PMMA, PS, PU, and PVDF, respectively (Table 4.7d). The order has identical results for Cu(I)-based surface impregnated composites as 3.59, 11.49, 15.87, and 20.51 mV (Table 4.7e).

One can conclude that the piezoelectric behaviour of TL crystals were verified by integrated crystalline particles into polymers and they show significant voltage change. Additionally, the combination of two piezoelectric materials cause the enhancement on the voltage change (PVDF/TL composite films). PU-based thin-film polymers than PMMA and PS shows the second better piezoelectricity towards the mechanical stress. This result may be originated the chemical affinity of PU with TL crystals due to nitrogen bonds and aromatic groups.

CHAPTER 5

CONCLUSION

Triboluminescence (TL) is known as the emission of light upon the application of any mechanical force. In order to develop stress responsive platform, these materials are the crucial compounds due to their self reporting mechano-sensing ability and optical properties. In term of generation sensing platform towards to compression force, TL materials which are EuD_4TEA and $Cu(NCS)(py)_2(PPh_3)$ were employed into transparent polymers. Two different process were carried out: i) embedding (or blending) and ii) surface impregnation and three transparent polymers: i) PMMA, ii) PS, iii) PU, and iv) PVDF were used for composite materials. Not only transparent films and nanofibers but also polymer beads were synthesized in order to develop TL/polymer composites. Drop tower mechanism allows to understand TL behaviour of composite materials and imaging technologies (AFM, SEM, FM, and oscilloscope) help to characterize the morphological and photophysical properties of composites.

It was conluded that the composites processing by surface impregnation method have TL response towards mechanical force in terms of two organometallic materials. The [TL] is determined as 2.5%. However, the composites processing by embedding (or blending) method have no TL response at this [TL]. When the concentration of TL materials is increased in the polymers, the embedded composites started to give TL response by the application of mechanical force. In the comparison of reproducibility of TL emission towards the number of ball shot, EuD_4TEA based composite has practically two times high durability than $Cu(NCS)(py)_2(PPh_3)$ based composites. For surface impregnated Eu(III)-based film composites, the results can be ordered as 7,11, 17, and 9 repeatation for PMMA, PS, PU, and PVDF respectively. Separately, for surface impregnated Cu(I)-based film composites, this order is 3, 5, 8, and 6 for PMMA, PS, PU, and PVDF respectively. When the nanofibers composites were taken into consideration, Eu(III)-based fiber composites can be ordered as 3, 4, 7, and 5 reproducibility and Cu-based fiber composites can be order as 2, 3, 4, and 3 for PMMA, PS, PU, and PVDF respectively. For this section, the overall outcome is that the TL/film composites are more appropriate to use them into mechano-sensing platform than TL/fiber composites.

Additionally, the synthesized of polymer beads have TL response. EuD_4TEA/PS NPs has single and sharp TL emission towards one ball shot; however, there is no reprodubility. Moreover, the heterogeneous media of EuD_4TEA/PS NPs causes to obtain lower emitted TL from composite than bulk EuD_4TEA crystals.

Piezoelectricity is the origin of the formation of triboluminescence behaviour. Lastly, the piezoelectric behaviour of thin-film polymer and thin-film composite were investigated. Among polymers which are used, only PVDF shows piezoelectricity due to producing high amount of electrical charge when it exposed to mechanical stress. The integration of crystalline particles into thin-film polymer allows to obtain piezoelectric response for each type composite with different values.

Overall, this study allows to understand TL materials, their composites by polymers for different end-use, and the behaviour of TL performance under different polymer media such as transparent film, nanofibers, and bead. This research is a way to generate mechano-sensing platform and control over TL emission in the polymer media.

REFERENCES

Acikgoz, M., and P. Gnutek. 2014. "Analysis of the zero-field splitting parameters of Mn^{2+} ions doped into yttrium aluminum borate YAl3(BO3)(4) single crystal: Substitution position of the impurity ion." *Optical Materials* 36 (8):1311-1318. doi: 10.1016/j.optmat.2014.03.021.

Ahn, Y., and J. Y. Son. 2016. "Mixed grains and orientation-dependent piezoelectricity of polycrystalline Nd-substituted Bi4Ti3O12 thin films." *Ceramics International* 42 (11):13061-13064. doi: 10.1016/j.ceramint.2016.05.086.

Akiyama, M., K. Nishikubo, and K. Nonaka. 2003. "Intense visible light emission from stress-activated SrMgAl6O11 : Eu." *Applied Physics Letters* 83 (4):650-652. doi: 10.1063/1.1594828.

Asefa, T., N. Coombs, H. Grondey, M. Jaroniec, M. Kruk, M. J. MacLachlan, and G. A. Ozin. 2002. "Bio-inspired nanocomposites: From synthesis toward potential applications." In *Advanced Biomaterials-Characterization, Tissue Engineering and Complexity*, edited by S. C. Moss, 347-357.

Bhunia, R., S. Das, S. Dalui, S. Hussain, R. Paul, R. Bhar, and A. K. Pal. 2016. "Flexible nano-ZnO/polyvinylidene difluoride piezoelectric composite films as energy harvester." *Applied Physics a-Materials Science & Processing* 122 (7). doi: 10.1007/s00339-016-0161-1.

Biju, S., Y. K. Eom, J. C. G. Bunzli, and H. K. Kim. 2013. "Biphenylene-bridged mesostructured organosilica as a novel hybrid host material for Ln(III) (Ln = Eu, Gd, Tb, Er, Yb) ions in the presence of 2-thenoyltrifluoroacetone." *Journal of Materials Chemistry C* 1 (21):3454-3466. doi: 10.1039/c3tc30459k.

Bunzli, J. C. G., A. S. Chauvin, H. K. Kim, E. Deiters, and S. V. Eliseeva. 2010. "Lanthanide luminescence efficiency in eight- and nine-coordinate complexes: Role of the radiative lifetime." *Coordination Chemistry Reviews* 254 (21-22):2623-2633. doi: 10.1016/j.ccr.2010.04.002.

Bunzli, J. C. G., and S. V. Eliseeva. 2013. "Intriguing aspects of lanthanide luminescence." *Chemical Science* 4 (5):1939-1949. doi: 10.1039/c3sc22126a.

Chandra, B. P. 1976. "KINETICS OF TRIBOLUMINESCENCE IN SUGAR CRYSTALS." *Indian Journal of Pure & Applied Physics* 14 (11):874-876.

Chandra, B. P., R. N. Baghel, A. K. Luka, T. R. Sanodiya, R. K. Kuraria, and S. R. Kuraria. 2009. "Strong mechanoluminescence induced by elastic deformation of rare-earth-doped strontium aluminate phosphors." *Journal of Luminescence* 129 (7):760-766. doi: 10.1016/j.jlumin.2009.02.015.

Chandra, B. P., V. K. Chandra, and P. Jha. 2015. "Modelling of fracto-mechanoluminescence damage sensor for structures." *Sensors and Actuators a-Physical* 230:83-93. doi: 10.1016/j.sna.2015.04.005.

Chandra, B. P., V. D. Sonwane, B. K. Haldar, and S. Pandey. 2011. "Mechanoluminescence glow curves of rare-earth doped strontium aluminate phosphors." *Optical Materials* 33 (3):444-451. doi: 10.1016/j.optmat.2010.10.014.

Chandra, V. K., and B. P. Chandra. 2012. "Dynamics of the mechanoluminescence induced by elastic deformation of persistent luminescent crystals." *Journal of Luminescence* 132 (3):858-869. doi: 10.1016/j.jlumin.2011.09.054.

Chen, H. J., S. J. Han, C. Liu, Z. H. Luo, H. P. D. Shieh, R. S. Hsiao, and B. R. Yang. 2016. "Investigation of PVDF-TrFE composite with nanofillers for sensitivity improvement." *Sensors and Actuators a-Physical* 245:135-139. doi: 10.1016/j.sna.2016.04.056.

Deepa, P., and M. Jayakannan. 2007. "Solvent-induced self-organization approach for polymeric architectures of micropores, hexagons and spheres based on polyurethanes prepared via novel melt transurethane methodology." *Journal of Polymer Science Part a-Polymer Chemistry* 45 (12):2351-2366. doi: 10.1002/pola.22058.

Demir, M. M., D. Soyal, C. Unlu, M. Kus, and S. Ozcelik. 2009. "Controlling Spontaneous Emission of CdSe Nanoparticles Dispersed in Electrospun Fibers of Polycarbonate Urethane." *Journal of Physical Chemistry C* 113 (26):11273-11278. doi: 10.1021/jp903899s.

Demir, M. M., I. Yilgor, E. Yilgor, and B. Erman. 2002. "Electrospinning of polyurethane fibers." *Polymer* 43 (11):3303-3309. doi: 10.1016/s0032-3861(02)00136-2.

Dickens, T., C. Armbrister, D. Olawale, and O. Okoli. 2015. "Characterization of triboluminescent enhanced discontinuous glass-fiber composite beams for micro-damage detection and fracture assessment." *Journal of Luminescence* 163:1-7. doi: 10.1016/j.jlumin.2015.02.030.

Eliseeva, S. V., D. N. Pleshkov, K. A. Lyssenko, L. S. Lepnev, J. C. G. Bunzli, and N. P. Kuzmina. 2011. "Deciphering Three Beneficial Effects of 2,2 '-Bipyridine-N,N '-Dioxide on the Luminescence Sensitization of Lanthanide(III) Hexafluoroacetylacetonate Ternary Complexes." *Inorganic Chemistry* 50 (11):5137-5144. doi: 10.1021/ic200450x.

Eliseeva, S. V., D. N. Pleshkov, K. A. Lyssenko, L. S. Lepnev, J. C. G. Bunzli, and N. P. Kuzminat. 2010. "Highly Luminescent and Triboluminescent Coordination Polymers Assembled from Lanthanide beta-Diketonates and Aromatic Bidentate O-Donor Ligands." *Inorganic Chemistry* 49 (20):9300-9311. doi: 10.1021/ic100974e.

Fontenot, R. S., K. N. Bhat, W. A. Hollerman, and M. D. Aggarwal. 2011. "Triboluminescent materials for smart sensors." *Materials Today* 14 (6):292-293.

Fontenot, R. S., K. N. Bhat, W. A. Hollerman, and M. D. Aggarwal. 2012. "Innovative triboluminescence study of multivitamin doped europium tetrakis." *Crystal Research and Technology* 47 (5):573-578. doi: 10.1002/crat.201100605.

Fontenot, R. S., K. N. Bhat, W. A. Hollerman, M. D. Aggarwal, and K. M. Nguyen. 2012. "Comparison of the triboluminescent yield and decay time for europium

dibenzoylmethide triethylammonium synthesized using different solvents." *Crystengcomm* 14 (4):1382-1386. doi: 10.1039/c2ce06277a.

Fontenot, R. S., W. A. Hollerman, K. N. Bhat, and M. D. Aggarwal. 2012. "Synthesis and characterization of highly triboluminescent doped europium tetrakis compounds." *Journal of Luminescence* 132 (7):1812-1818. doi: 10.1016/j.jlumin.2012.02.027.

Fontenot, R. S., W. A. Hollerman, K. N. Bhat, and M. D. Aggarwal. 2013. "Effects of added uranium on the triboluminescent properties of europium dibenzoylmethide triethylammonium." *Journal of Luminescence* 134:477-482. doi: 10.1016/j.jlumin.2012.07.042.

Fontenot, R. S., W. A. Hollerman, K. N. Bhat, M. D. Aggarwal, and B. G. Penn. 2014. "Incorporating strongly triboluminescent europium dibenzoylmethide triethylammonium into simple polymers." *Polymer Journal* 46 (2):111-116. doi: 10.1038/pj.2013.78.

Fontenot, Ross S., William A. Hollerman, Kamala N. Bhat, Stephen W. Allison, and Mohan D. Aggarwal. 2013. "Luminescent properties of lanthanide dibenzoylmethide triethylammonium compounds." *Journal of Theoretical and Applied Physics* 7 (1):1-10. doi: 10.1186/2251-7235-7-30.

Gusarov, B., E. Gusarova, B. Viala, L. Gimeno, and O. Cugat. 2016. "PVDF piezoelectric voltage coefficient in situ measurements as a function of applied stress." *Journal of Applied Polymer Science* 133 (14). doi: 10.1002/app.43248.

Hasegawa, Y., and T. Nakanishi. 2015. "Luminescent lanthanide coordination polymers for photonic applications." *Rsc Advances* 5 (1):338-353. doi: 10.1039/c4ra09255d.

Hollerman, W. A., R. S. Fontenot, K. N. Bhat, M. D. Aggarwal, C. J. Guidry, and K. M. Nguyen. 2012. "Comparison of triboluminescent emission yields for 27 luminescent materials." *Optical Materials* 34 (9):1517-1521. doi: 10.1016/j.optmat.2012.03.011.

Jain, A., K. J. Prashanth, A. K. Sharma, A. Jain, and P. N. Rashmi. 2015. "Dielectric and piezoelectric properties of PVDF/PZT composites: A review." *Polymer Engineering and Science* 55 (7):1589-1616. doi: 10.1002/pen.24088.

Jha, P., and B. P. Chandra. 2014. "Survey of the literature on mechanoluminescence from 1605 to 2013." *Luminescence* 29 (8):977-993. doi: 10.1002/bio.2647.

Jin, X., M. Gotz, S. Wille, Y. K. Mishra, R. Adelung, and C. Zollfrank. 2013. "A Novel Concept for Self-Reporting Materials: Stress Sensitive Photoluminescence in ZnO Tetrapod Filled Elastomers." *Advanced Materials* 25 (9):1342-1347. doi: 10.1002/adma.201203849.

Khalil, G. E., K. Lau, G. D. Phelan, B. Carlson, M. Gouterman, J. B. Callis, and L. R. Dalton. 2004. "Europium beta-diketonate temperature sensors: Effects of ligands, matrix, and concentration." *Review of Scientific Instruments* 75 (1):192-206. doi: 10.1063/1.1632997.

Lawson, C., A. Stanishevsky, M. Sivan, P. Pokorny, and D. Lukas. 2016. "Rapid fabrication of poly(epsilon-caprolactone) nanofibers using needleless alternating current

electrospinning." *Journal of Applied Polymer Science* 133 (13). doi: 10.1002/app.43232.

Link, S., and M. A. El-Sayed. 2000. "Shape and size dependence of radiative, non-radiative and photothermal properties of gold nanocrystals." *International Reviews in Physical Chemistry* 19 (3):409-453. doi: 10.1080/01442350050034180.

Marchetti, F., C. Di Nicola, R. Pettinari, I. Timokhin, and C. Pettinari. 2012. "Synthesis of a Photoluminescent and Triboluminescent Copper(I) Compound: An Experiment for an Advanced Inorganic Chemistry Laboratory." *Journal of Chemical Education* 89 (5):652-655. doi: 10.1021/ed2001494.

Mayuri, P. V., and P. Ramesh. 2016. "Fabrication and characterization of silver nanoparticle impregnated uniaxially aligned fibre yarns by one-step electrospinning process." *Journal of Materials Science* 51 (5):2739-2746. doi: 10.1007/s10853-015-9587-7.

Mei, Z. X., X. Q. Zhang, Z. G. Yao, J. M. Han, and J. Z. Li. 2001. "Study on the triboluminescent property of ZnS : Mn." *Spectroscopy and Spectral Analysis* 21 (6):766-768.

Meuer, S., and R. Zentel. 2008. "Functional diblock copolymers for the integration of triboluminescent materials into polymer matrices." *Macromolecular Chemistry and Physics* 209 (2):158-167. doi: 10.1002/macp.200700291.

O'Hara, P. B., C. Engelson, and W. St Peter. 2005. "Turning on the light: Lessons from luminescence." *Journal of Chemical Education* 82 (1):49-52.

Olawale, D. O., T. Dickens, W. G. Sullivan, O. I. Okoli, J. O. Sobanjo, and B. Wang. 2011. "Progress in triboluminescence-based smart optical sensor system." *Journal of Luminescence* 131 (7):1407-1418. doi: 10.1016/j.jlumin.2011.03.015.

Oliveira, C. K., V. P. de Souza, L. L. da Luz, J. R. D. Vicenti, R. A. Burrow, S. Alves, R. L. Longo, and I. Malvestiti. 2016. "Synthesis, crystal structure and luminescent properties of lanthanide extended structure with asymmetrical dinuclear units based on 2-(methylthio)benzoic acid." *Journal of Luminescence* 170:528-537. doi: 10.1016/j.jlumin.2015.06.037.

Pu, X., L. X. Li, H. Q. Song, C. H. Du, Z. F. Zhao, C. Y. Jiang, G. Z. Cao, W. G. Hu, and Z. L. Wang. 2015. "A Self-Charging Power Unit by Integration of a Textile Triboelectric Nanogenerator and a Flexible Lithium-Ion Battery for Wearable Electronics." *Advanced Materials* 27 (15):2472-2478. doi: 10.1002/adma.201500311.

Raja, S. N., A. C. K. Olson, K. Thorkelsson, A. J. Luong, L. Hsueh, G. Q. Chang, B. Gludovatz, L. W. Lin, T. Xu, R. O. Ritchie, and A. P. Alivisatos. 2013. "Tetrapod Nanocrystals as Fluorescent Stress Probes of Electrospun Nanocomposites." *Nano Letters* 13 (8):3915-3922. doi: 10.1021/nl401999t.

Reddy, D. R., and B. K. Reddy. 2002. "Laser-like mechanoluminescence in ZnMnTe-diluted magnetic semiconductor." *Applied Physics Letters* 81 (3):460-462. doi: 10.1063/1.1494116.

Rieger, K. A., N. P. Birch, and J. D. Schiffman. 2016. "Electrospinning chitosan/poly(ethylene oxide) solutions with essential oils: Correlating solution rheology to nanofiber formation." *Carbohydrate Polymers* 139:131-138. doi: 10.1016/j.carbpol.2015.11.073.

Seminara, L., M. Capurro, P. Cirillo, G. Cannata, and M. Valle. 2011. "Electromechanical characterization of piezoelectric PVDF polymer films for tactile sensors in robotics applications." *Sensors and Actuators a-Physical* 169 (1):49-58. doi: 10.1016/j.sna.2011.05.004.

Sinha, T. K., S. K. Ghosh, R. Maiti, S. Jana, B. Adhikari, D. Mandal, and S. K. Ray. 2016. "Graphene-Silver-Induced Self-Polarized PVDF-Based Flexible Plasmonic Nanogenerator Toward the Realization for New Class of Self Powered Optical Sensor." *Acs Applied Materials & Interfaces* 8 (24):14986-14993. doi: 10.1021/acsami.6b01547.

Souza, E. R., Jhsk Monteiro, I. O. Mazali, and F. A. Sigoli. 2016. "Photophysical studies of highly luminescent europium(III) and terbium (III) complexes functionalized with amino and mercapto groups." *Journal of Luminescence* 170:520-527. doi: 10.1016/j.jlumin.2015.03.032.

Sun, C. Q., S. Li, and B. K. Tay. 2003. "Laser-like mechanoluminescence in ZnMnTe-diluted magnetic semiconductor (vol 81, pg 460, 2002)." *Applied Physics Letters* 82 (20):3568-3569. doi: 10.1063/1.1576890.

Teotonio, E. E. S., G. M. Fett, H. F. Brito, W. M. Faustino, G. F. de Sa, Mcfc Felinto, and R. H. A. Santos. 2008. "Evaluation of intramolecular energy transfer process in the lanthanide(III) bis- and tris-(TTA) complexes: Photoluminescent and triboluminescent behavior." *Journal of Luminescence* 128 (2):190-198. doi: 10.1016/j.jlumin.2007.07.005.

Welsh, J. P., K. G. Patel, K. Manthiram, and J. R. Swartz. 2009. "Multiply mutated Gaussia luciferases provide prolonged and intense bioluminescence." *Biochemical and Biophysical Research Communications* 389 (4):563-568. doi: 10.1016/j.bbrc.2009.09.006.

Xu, C. N., H. Yamada, X. S. Wang, and X. G. Zheng. 2004. "Strong elasticoluminescence from monoclinic-structure SrAl2O4." *Applied Physics Letters* 84 (16):3040-3042. doi: 10.1063/1.1705716.

Yu, J. H., C. C. Zhang, L. Ge, P. Dai, and S. G. Ge. 2009. "Quantification of Sorbic Acid Using the Molecularly Imprinted Chemiluminescence Method with Rhodanine Derivative." *Analytical Sciences* 25 (11):1351-1356.